Accepted manuscript – Accepted by *Structures* on 20/08/2022

A review of WAAM for steel construction – manufacturing, material and geometric properties, design, and future directions

Sian I. Evans[a], Jie Wang[a,*], Jian Qin[b], Yongpeng He[a], Paul Shepherd[a], Jialuo Ding[b]

[a] Department of Architecture and Civil Engineering, University of Bath, Bath, BA2 7AY

[b] Welding Engineering and Laser Processing Centre, School of Aerospace Transport and Manufacturing, Cranfield University, Cranfield, MK43 0AL

[*] Corresponding author: j.wang@bath.ac.uk

Abstract

This paper provides a review of the capabilities of WAAM for manufacturing steel components for use in the construction industry, with a focus on the structural stability and design of WAAM builds. Manufacturing techniques that can be used for WAAM construction are first discussed. This is followed by a detailed review of the material and geometric properties, and the resulting structural stability performance of WAAM steel structures to date. To exploit the advantage of WAAM in building free-form shapes, structural optimisation techniques suitable for WAAM construction are discussed. Lastly, conclusions and future research directions are provided.

Keywords: *Wire arc additive manufacturing (WAAM), Additive manufacturing (AM), Manufacturing parameters, Material properties, Geometry*

1.0 Introduction

3D printing, and in particular Wire Arc Additive Manufacturing (WAAM, otherwise known as Wire Arc Direct Energy Deposition (WA-DED)), is transforming the construction industry [1]. Amongst other metal additive manufacturing (AM) technologies, WAAM has been identified as the most suitable process for AM steel construction, due to its relatively high deposition rate (4-9 kg/hr for steel compared to 50 g/hr for powder bed fusion [2]), low cost [3] and unlimited build size [4]. It is also a favourable technique as no powder recycling system is needed, and a vacuum is not required (saving vacuum creation time) unlike with powder bed fusion and e-beam DED respectively [5], [6].

Initially developed for mechanical applications, WAAM is a material efficient alternative to subtractive techniques [7], [8]. Whilst 52% of global steel is used for construction as reinforcement bars, plates and structural profiles which are traditionally rolled or welded into standard or universal prismatic shapes [9], on average, half of steel in structures is not used to bear design loads [10] because shear forces and bending moments aren't constant along the length of a member [11]. By employing WAAM, more structurally efficient, non-prismatic, free-formed geometries are made possible. Additionally, combinations of alloys can be used to produce functionally graded materials [12], and parts can be produced with variable microstructures by controlling cooling rates, which can lead to advantageous material properties [13].

Use of WAAM in construction could increase automation, reducing physical workload and improving workplace safety [14]. Furthermore, it could allow safer construction in harsh environments such as war zones, areas affected by natural disasters, and extra-terrestrial sites [15]. Trusses with optimised cross-sections and free form joints have been realised using WAAM, and the design efficiency (using capacity-to-mass ratio) was found to be at least

double that of conventional designs (Figure 1a [16] and Figure 1b [17]). This highlights how WAAM could be used to manufacture material efficient designs that cannot be produced using conventional processes [16]. Two steel footbridges (one in Darmstadt, Germany (Figure1c [18]) and one in Amsterdam, The Netherlands (Figure 1d) [19]) have also been successfully manufactured using WAAM [19], with the former being manufactured in situ. However, there are still significant research gaps in establishing the optimal process parameters to be used, and whether the mechanical properties and structural stability of WAAM steel structures meet the design requirements for other civil applications. To this end, this paper provides a detailed review of the potential use of WAAM to produce steel members for use in construction and identifies the research gaps and areas of opportunities.

Figure 1: Successful examples illustrating the potential of WAAM in steel construction. a) Truss structure with optimised member sizes [16]; b) connection of spatial shells [17]; c) the bridge in Darmstadt [18]; d) MX3D bridge in Amsterdam (Photo taken by the authors). Reprinting permission for these images has been obtained from the publishers[16]–[18].

Many review papers covering WAAM focus on aluminium or titanium alloys and their applicability to industries such as the aerospace industry, automobile industry and marine industry [16]–[19]. In fact, Ti-6Al-4V is the most popular material investigated for use with WAAM technology [20]. However, these metals are a lot more expensive than other material options such as steel, so they are not the preferred metals for the construction industry [21]. Other review papers focus on the automation of WAAM, path planning, and sensing/controlling during building [17], [18], [20], [22]. Ancillary processing of components made by WAAM has also been reviewed, including heat treatment, hot isostatic pressing (HIPing), and shot peening [17], [23]–[25]. These post-processing methods are used to reduce the degree of defects such as residual stresses, distortion and porosity, which have been reviewed in other papers [17]–[19], [23], [25]–[27]. Post-processing has been identified as the third most significant cost-driver in WAAM [20], however, tolerances on manufacturing defects may be larger for the construction industry than those for the automotive and aerospace engineering industries, meaning that these expensive processes may be avoided in construction [28]. This is beneficial as the large parts used in the construction industry could take a long time to post-process, and in the case of heat treatment, may require large furnaces [29]. The topic of 3D printing in the construction industry has been reviewed [2], [8], [9], [30], but in a broad sense, not limited to metal feedstock or WAAM. Kuhne et al. have analysed WAAM in construction [31], however, this conference paper is not exhaustive and therefore, a more detailed review is carried out in this paper. Whilst the microstructure of WAAM parts has been reviewed [21], there is yet to be a comprehensive review on their structural properties.

In the current paper, a description of the WAAM process and emerging technologies suitable for construction are first introduced. The material properties and types of geometric imperfections of WAAM structures, along with the effects of different manufacturing parameters on them, are then reviewed. This is followed by a discussion on topology

optimisation and structural form-finding methods that may benefit WAAM construction. The final section discusses the current inconsistencies in findings, identifies the research gaps and provides suggestions for future research directions for the development of WAAM in the construction industry.

2.0 WAAM technologies for construction

2.1 Introduction

WAAM is a type of direct energy deposition (DED) in which metal wire is fed into an electric arc and is then selectively deposited to form the part being manufactured [3] (Figure 2a). Metal Inert Gas (MIG), Tungsten Inert Gas (TIG) or Plasma Arc (PA) technology can be used to produce the electric arc (see Section 2.2), and the motion can be controlled by either a robotic system or computer numerical-controlled (CNC) gantries [22]. CNC gantries are more stiff and accurate than robotic systems, but robotic systems can be used in parallel to achieve greater deposition rates, and are manoeuvrable, making them suitable for very large builds [23]. There is virtually no limit on the size of the part produced by robotic systems [4] so large structural elements are possible to manufacture, making WAAM a suitable process for the construction industry. In comparison, the size of a part produced by powder bed fusion (PBF) is constrained to the size of the powder bed (usually 250 × 250 × 250 mm^3) [2]. DED has a much higher deposition rate than other AM techniques, however, the surface quality and dimensional accuracy are inferior [24], meaning that subtractive post-processing is often required to ensure the part meets the requirements for geometric accuracy [25]. This must be avoided in construction due to the scale of the parts and the accessibility of the faces [26].

WAAM is less expensive than other methods of metal AM (including PBF) due to the fact that the equipment is off-the-shelf, the technology is more mature [3] and the feedstock costs 10% that of powder [27]. Whilst some of this cost saving may be offset in cases where the surface

waviness needs to be machined off after manufacture to give an appropriate surface finish [28], WAAM can still offer cost savings when compared to machining a part from solid [8]. In the construction industry, parts are subject to relatively more static and predictable loading cases than in Mechanical Engineering, and therefore, WAAM builds for use in construction may be subjected to less restrictive requirements on geometric accuracy, reducing the need to machine their surfaces. This is seen in previous studies [19], [29], where surface machining was omitted when producing WAAM structures for civil applications.

Thin-walled structures are traditionally used in construction, as a compromise between structural capacity and material usage, however, this can lead to instability issues. WAAM could be used to produce parts with beneficial imperfections which could improve the plate buckling resistance [30]. WAAM may also provide a method for realising complex, doubly-curved geometries such as shells [31].

Another benefit of WAAM is that wire is a preferable feedstock when compared to powder because it is easier to store and handle as it poses fewer hazards associated with the environment and health and safety [32]. In DED, a protective gas (such as argon) is used to prevent oxidation [33] as this may lead to oxidised impurities acting as brittle phases, which could become initiation points of cracks [27]. Since wire has less surface area per kilogram when compared to powder, it is less likely to oxidise or be contaminated to the same extent [34] and therefore wire processes (such as WAAM) are preferrable.

Unfortunately, structures produced by AM generally are subjected to large residual stresses which can result in geometric inaccuracy and large distorsion. This is particularly an issue for WAAM, as WAAM usually works for much larger scale parts so the distortions/accumulated stresses make more trouble [35], making the designing of WAAM structures more complex. Often the scale of the distortion is only evident once the substrate has been detached from the bed [36] and it is caused by both the excessive heat input and the high deposition rate [37].

Whilst WAAM is best suited for applications with low to medium complexity, this is acceptable for the construction industry so this does not pose such a large drawback [4]. Printing can be performed in continuous or dot-by-dot mode; as most structural elements are planar rather than line elements, continuous printing is the usual mode used for construction purposes [22]. For this mode, the deposition direction and build direction are as described in Figure 2b.

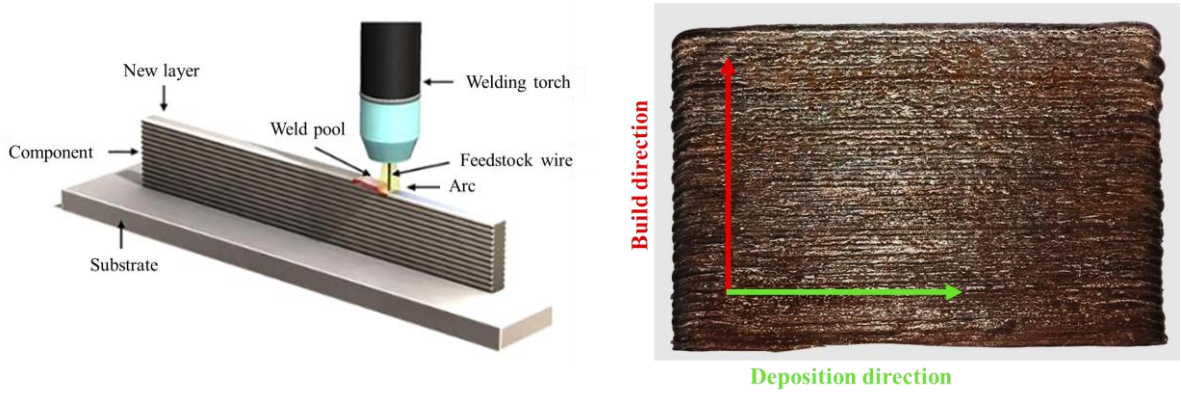

a) Schematic of WAAM (reprinting permission for these images has been obtained from the publishers [38]).

b) Orientation of build and deposition directions (image by authors).

Figure 2: WAAM schematics.

2.2 Types of electric arc

There are three main types of electric arc used for WAAM; MIG, TIG and PA. MIG is the usual process of choice as the wire is the consumable electrode, meaning that it is coaxial with the welding torch, which results in a simpler tool path. In the case of TIG or PA welding, the electrode is non-consumable, and an external wire must be fed into the melt pool. Here, the torch must be able to rotate to allow the wire to always be fed from the same direction to ensure consistent deposition, making the programming aspect of manufacture more complicated [4]. In MIG, the metal is transferred from the consumable electrode, through the arc, to the melt pool. This results in spatter as some molten droplets are ejected from the arc or weld pool, often

creating balling on the surface of the build (see Section 4.5). In TIG and PA, the filler metal is delivered directly to the weld pool so these processes are not susceptible to spatter [39].

Cold Metal Transfer (CMT) is a modified MIG variant suitable for use with aluminium and steel feedstocks [4]. It can produce high quality beads with close to no spatter, and with a lower heat input, due to the fact that it uses a controlled dip transfer mode mechanism. The lower heat input results in finer grains, which can improve the mechanical properties [40]. It is distinguished from conventional MIG because the electrical process control that senses arc length, the short circuiting phase and the thermal input, is synchronised with mechanical motion of the wire [41]. Further details can be found in [40]–[42].

As the parts required for construction are large, a high deposition rate is required to produce the parts in a reasonable timeframe. MIG usually has the greatest deposition rate (several kilograms per hour, compared to approximately 1 kg/h for TIG) so it is the preferred method in the construction industry [40]. Therefore, previous research into WAAM construction is mainly focused on MIG and this may have narrowed the application scope of this technology. Other WAAM variants may also be worth attention from civil engineers for different structural applications; for example, TIG could be used when greater geometric precision and superior surface finish is required [40], and PA could be used to build parts with a wider deposition width than that of MIG [43].

2.3 Control of geometry

WAAM processes are well known for their high deposition rate, however they are accompanied with poorer part accuracy and more challenges in geometry control compared to other AM processes (e.g. laser-based processes). Geometry control often governs the selection of process parameters in practice and has been one of the major research focuses for WAAM. The prediction and control of the dimension of each layer (i.e. height and width) has been studied

for a range of metallic materials [44]–[49]. The wall thickness and deposition efficiency of a single-pass deposition relies primarily on the wire thickness and the process parameters (including heat input, wire-feeding speed, and travel/scanning speed). For constructional materials such as stainless and carbon steels, 0.8 mm – 1.2 mm wires are most often used, allowing section thicknesses ranging from 3.5 mm to 8 mm for a single-pass wall [35], [50], [51]. In construction applications to date, WAAM builds have mostly adopted single-pass walls with a constant thickness [19].

Thicker walls may be achieved through multi-wire feeds [52]–[57] and multi-pass prints, adding further complications in path-planning [58]. The wall thickness may be also varied via a hybrid DED process [59], where plasma transferred arc (PTA) is used as the main energy source to generate the melt pool, and a laser is applied for controlling the layer width, enabling a smooth and accurate variation of wall thickness. This hybrid process can achieve significantly faster deposition rates than both pure arc and pure laser-based additive manufacturing processes (i.e. 2.2 times the deposition rate of a pure laser process and 1.7 times that of a pure arc process) whilst using the same energy input [59] and whilst controlling the geometry. There is great research potential in exploring more combinations of the different energy sources to achieve various required targets [60].

Monitoring of traditional welding parameters (e.g. arc voltage, arc current, wire feed speed, travel speed and shielding gas flow) alone is insufficient as these are only associated with the system and not the component; environment conditions, such as heat accumulation, must be considered too. Different types of monitoring are described in [36], including acoustic signal, x-ray CT, optical signal and thermal signal. As defects can accumulate, their consequences may be severe. In-situ monitoring and control are required to resolve defects as they occur [36].

The geometric accuracy of WAAM parts essentially relies on prediction and control of the dimension of each layer, which is affected by a considerable number of process parameters and

the combined effects of them. Ding et al. [61] proposed one of the earliest digital modelling solutions for determining suitable process parameters. In [61], the thermo-mechanical behaviour of the multi-layer wall structure during the WAAM process was simulated using finite element analysis to predict the accumulated residual stress and distortion. Xiong et al. [62] have investigated the deposition geometry prediction and control of the GMAW-based WAAM process, where neural network modelling was applied as the deposition geometry prediction algorithm and a closed-loop iteration system was developed to optimise the process parameters. The digital modelling approach has built significant confidence in residual stress analysis and geometric control of WAAM parts. For different materials the effects of process parameters can vary. It imposes a great challenge for engineers to collect the process knowledge from numerous experimental and numerical data available in literature. For this reason, machine learning employing digital technologies [63] may be adopted for optimising the process parameters to achieve the desired geometry. In [63], a digital tool for collecting data within numerous literatures was developed, proven to be applicable for data-driven process control in additive manufacturing.

2.4 Slicing and path planning

The structural design of WAAM parts may be constrained by manufacturing feasibility, including minimising the number of starts and stops of the power source to maintain a continuing process with one trajectory [64], minimising the angle of overhangs [16], [65], positioning the welding torch without contacting the AM parts [16], and overcoming T-junctions or X-junctions [58].

Parts with relatively straight forward cross-sectional shapes produced by a single wall pass (e.g. manufacturing CHS, SHS, and the MX3D bridge [3], [16], [19], [29], [51], [66]) can be manufactured in a continuous manner. In the first end-to-end framework developed for

building WAAM tubular trusses [16], the path planning was determined by grouping similar geometric features to be manufactured with the same printing strategy, minimising the amount of substrate reorientation and keeping the building direction as vertical as possible (Figure 3a). The feasibility of the selected printing process was then confirmed by simulating all the steps in the virtual environment of Metal XL using slicing and kinematic analysis [16].

For thin-walled geometries with high degrees of 3D curvatures, the traditional path planning approach is based on uniform slicing [16]. Diourte et al. [64] proposed an alternative strategy named the continuous three-dimensional path planning (CTPP) based on 'adaptive slicing' (Figure 3b), where each slice consists of a different layer height. This method efficiently reduces the number of arc starts and stops and has been tested successful in manufacturing two thin-walled parts using the CMT process [64].

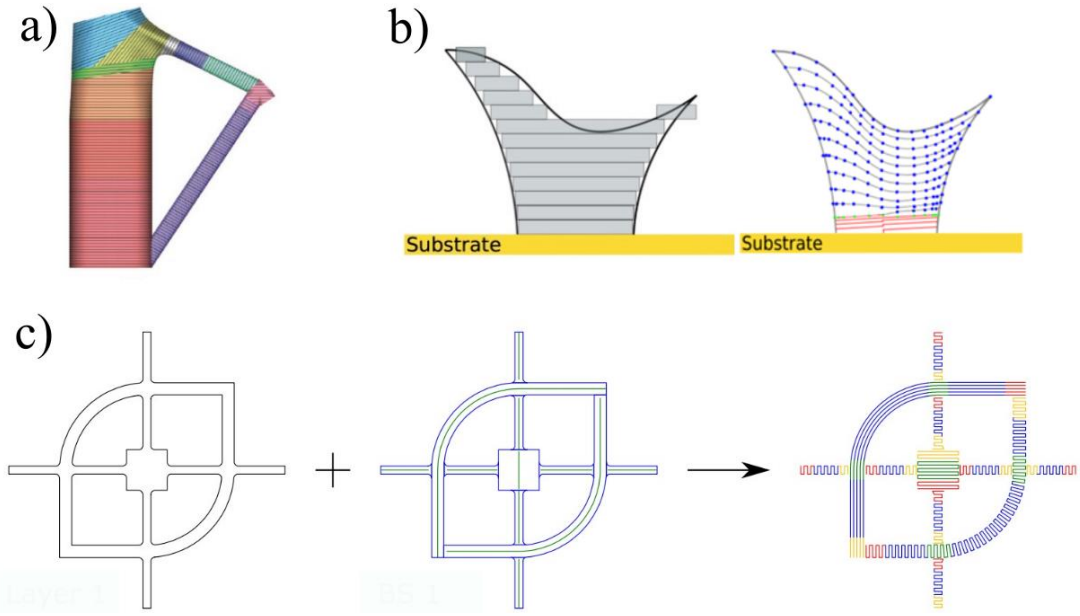

Figure 3: Typical path planning methods suitable for WAAM construction: a) Uniform slicing method in conjunction with 5-axis printing [16]; b) Uniform slicing (discontinuous trajectory) vs adaptive slicing method (continuous trajectory) [64]; c) Modular path planning for thicker and more complexed geometries [58] (Reprinting permission for these images has been obtained from the publishers [16], [58], [64]).

More complexed structural geometries with varying wall thicknesses and interconnections can be manufactured by WAAM using the modular path planning solution, as proposed by Michel et al. [58] (Figure 3c). In this method, variation of wall thicknesses is achieved by using parallel or oscillated scanning strategy; each layer was segmented into different modules based on its geometric feature, the manipulator trajectory was then determined based on its feasibility at the interconnections. The process parameters of every segment were determined based on processing knowledge. This was the first time that processing knowledge was integrated into the path planning, and it has been shown to generate WAAM parts with fewer defects [58]. Further information on path planning techniques such as raster, contour, spiral, continuous, hybrid and medial axis transformation can be found in [67].

2.5 Machining of WAAM

Whilst it is not desirable to machine the surface of large WAAM structures for use in the construction industry (due to the size of the parts, the cost involved, the volume of material wasted, and internal surfaces which cannot easily be machined), milling may be used for smaller structural connections. However, the thin-walled structures often produced with WAAM pose difficulties when it comes to machining their surfaces; the thin sections are prone to forced vibrations, chatter, and deflection issues. These difficulties are usually overcome by reducing the material removal rate; however, this reduces productivity. The dynamic behaviour of thin-walled pieces during milling needs to be studied further, with an approach given by Grossi et al. [68].

Lopes et al. [69] have found that the surface improves with an increased cutting speed and a decreased feed per tooth, but further research is required to establish the optimum strategies for decreased tool wear, whilst maintaining high surface quality and high productivity.

Machining can be done as a separate step, on a separate machine to the printing, but cooperative systems and hybrid additive-subtractive processes, which include WAAM and machining in the same system, have been developed [70]–[72]. The effects of machining WAAM builds on its material properties are detailed in the relevant sub-sections in Section 3.0.

2.6 Concluding remarks

It is clear that WAAM is a suitable technology for producing parts with the dimensions and geometries required for construction; further details on its ability to produce parts with the required material properties can be found in Section 3. However, as with all manufacturing techniques, there are both benefits and drawbacks to WAAM, as highlighted in 2.1. Whilst it has been suggested that combining different electric arcs may be beneficial for achieving a larger range of geometries, the practicalities involved (such as additional build time, cost, and complexity of the equipment) must be evaluated in more detail in order to assess the overall benefit achieved. Given the infinite number of combinations of slicing and path planning techniques, standards must be created for design, manufacture, and quality assurance, to ensure that WAAM parts built for construction meet the tolerances on geometry, whilst improvements in process control will help. The challenge of manufacturing large parts on site, without rotating them, has already gained attention [18], and further progress is expected in future years.

3.0 Material properties and influence of processes

The structural performance of steel structures is highly dependent on their material properties such as Young's modulus, yield and tensile strengths, ductility, and fatigue resistances. These material properties have been very well studied for traditionally manufactured steel structures, where standardized manufacturing methods (i.e. hot-rolling, cold-forming and welding) have been established and corresponding design guidelines have been developed. For WAAM components, these material properties are highly variable as there is no established set of

WAAM manufacturing parameters designed specifically for structural applications. Therefore, this section provides a review of the key material properties of WAAM steel structures and discusses how they vary with changes to the manufacturing parameters. A list of tensile material tests of stainless and carbon steels made by WAAM is summarised in Table 1, with information on material grade, angle of extraction, printing parameters used, and post-processing methods employed.

Table 1: Details of tensile tests carried out in literature on carbon steel and stainless steel WAAM samples.

Steel Grade	**No. of tests**	**Angle (°) of extraction**	**Details**
308LSi [73]	12 M*; 39 AB**	0, 45, 90	WFS 4-8 m/min.
304L [74]	6 M	0, 90	WFS 1 m/min; average results reported only.
304L [75]	9 M	0, 45, 90	Active cooling used; WFS 4-8 m/min.
308LSi [3]	6 M	0, 45, 90	Initial voids detected.
ER70S-6 [76]	8 M; 14 AB	0, 45, 90	Average results reported only.
308LSi [29]	2 M; 8 AB	0, 45, 90	WFS 0.6-2 m/min.
308LSi [31]	2 M; 9 AB	0, 90	Porosity thought to be detected.
ER70S-6 [38]	8 M	0, 45, 90	MIG.
308L [77]	6 M	0, 90	MIG with variable WFS; 40 s dwell time.
304L [78]	7 M	0, 90	Average results reported only.
316LSi [35]	24 M	0, 90	WFS 2 m/min; Different combinations of heat input and interpass temperature used; average results reported only.
308LSi [50]	12 M; 32 AB	0, 90	WFS 4-8 m/min; active and uncontrolled cooling used; graphical results reported only.
316L [79]	6 M	0, 90	WFS 2 m/min; in-process cryogenic cooling compared to interpass temperature control; graphical results reported only.
304 [80]	8 M	0	WFS 5.4 m/min; graphical results reported only.
ER70S [80]	7 M	0, 90	WFS 5.1 m/min; graphical results reported only.
316L & 316LSi [81]	~100 M	0, 90	Combinations of different heat inputs, cooling strategies and deposition rate used. Graphical results reported only.

ER70S-6 [82]	24 M	0, 90	WFS 8 m/min. Different path planning strategies used. Average results reported only.
ER70S-6 [83]	6 M	0, 90	Dwell period of 60 s.
ER70S-6 [84]	4 M	0, 90	Average results reported only.
ER100S-1 [84]	4 M	0, 90	Average results reported only.

*M – machined

**AB – as-built

3.1 Microstructure

The material properties of a WAAM structure are significantly affected by its microstructure [85], which can be similar to that of welds. However, different printing strategies (e.g. parallel path or alternating scan direction) may lead to variations in the microstructure. In typical welds, the grains grow towards the centreline of the melt pool, however, when the scan direction is altered between layers during AM, the grains can grow more upright [86]. The microstructure is usually complex and so cannot be characterised by a single grain size number [78].

Stainless steels are the most studied alloys used for WAAM construction and they usually have a columnar microstructure when produced by AM; an equiaxed microstructure is rarely seen due to the high temperature gradients found in WAAM. The forged substrate that the part is built on has equiaxed grains of random orientation and the first layer of the AM part is melted on top of this. As the current layer has the same chemical composition as the previous layer (or substrate, in the case of the first layer), nucleation of a new phase is not required [87] so the grains grow epitaxially. When the second layer is deposited, there is preferred growth due to temperature gradients (substantially downwards due to the substrate and previous layers acting as a heat sink) and the grains grow vertically in the build direction via competitive growth, leading to an anisotropic microstructure [88]. This can produce anisotropic mechanical properties [89] which can be detrimental for applications involving multidirectional stresses, so an aligned columnar grain structure is not appropriate in these situations [90]. Equiaxed grain materials generally exhibit higher strength and a constant strain hardening rate, whereas

columnar grain materials show a progressively increasing strain hardening rate with increasing true strain [91]. Therefore, Liu et al. have investigated the columnar to equiaxed transition (CET) to achieve the more favourable properties exhibited by equiaxed grains [92].

3.2 Young's modulus

The Young's modulus of WAAM stainless steels has been found to be affected by the angle of testing to the build direction, surface post-processing, and manufacturing parameters including the heat input and interpass temperature [3], [73], [75], [78]. Whilst a higher heat input has been shown to achieve a greater Young's modulus than that of a lower heat input, WAAM generally produces stainless steel structures with a Young's modulus less than that of wrought and annealed material ([35] and Figure 4a).

Some authors have found that the Young's modulus of a WAAM tensile coupon sample is affected by the angle at which it is extracted. In the case of stainless steel samples which have been milled flat, coupons taken at an angle of 45° to the build direction have been found to have the highest Young's modulus, whereas samples taken at 0° and 90° have been found to have lower Young's moduli [3], [73]. In contrast, Laghi et al. [75] have found that there is no significant difference between the Young's moduli of milled stainless steel samples taken at different angles.

The undulating geometry of as-built stainless steel samples has been found to reduce the Young's modulus by 20-35% when compared to milled samples [19], [73], with thinner as-built samples being most affected because the magnitude of the undulations is greater relative to the thickness of the section [73]. This is particularly relevant to the construction industry where builds are not expected to have their surfaces milled all over, due to the monetary and time costs associated with post-processing large components.

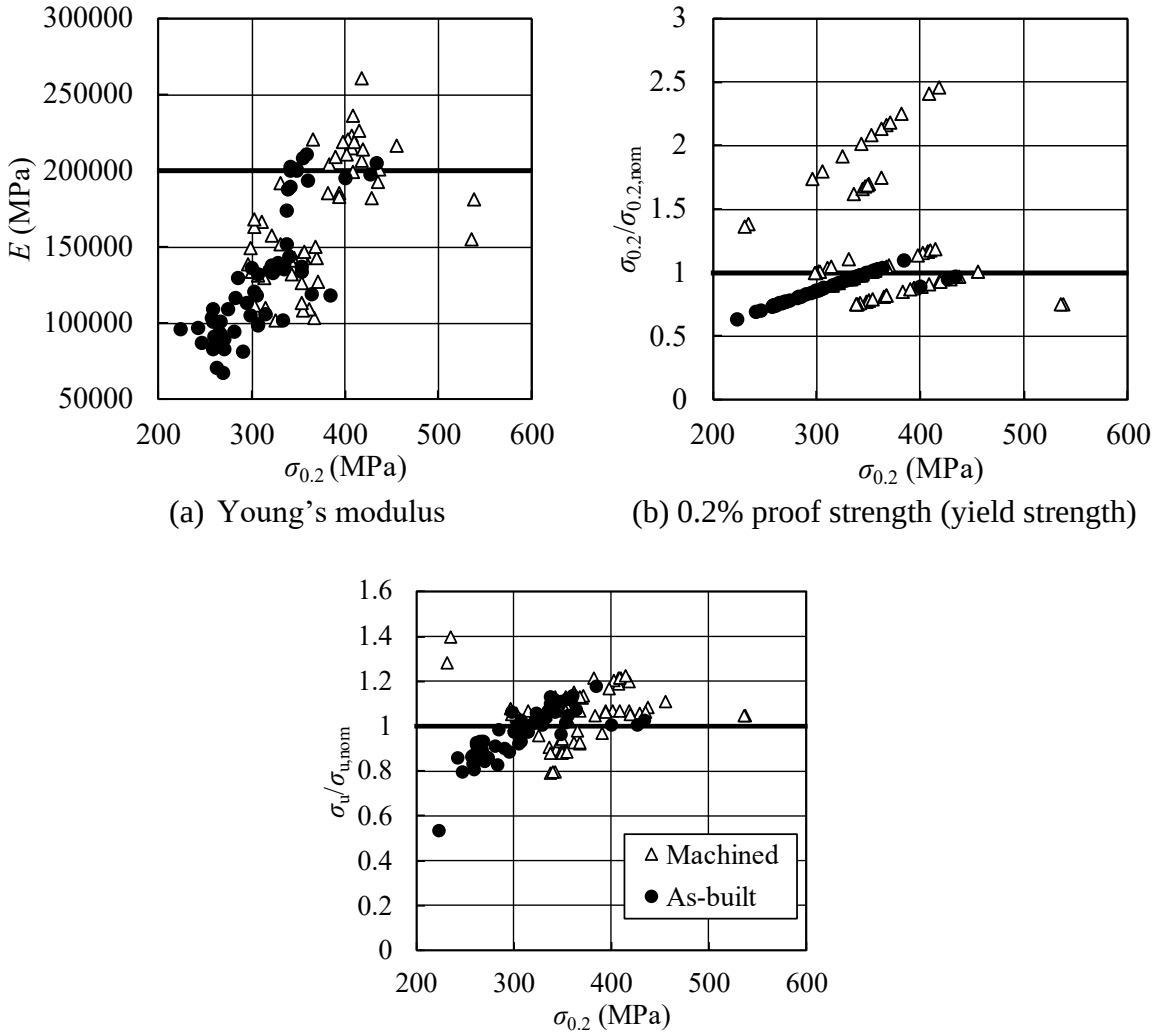

(a) Young's modulus

(b) 0.2% proof strength (yield strength)

(c) Ultimate tensile strength

Figure 4: Collected tensile coupon test data of stainless steel and carbon steel made by WAAM [3], [29], [31], [35], [38], [73]–[78], [82]–[84], [93]–[96]. Permission to use this data has been obtained from the publishers

341

342 **3.3 Yield Strength and Ultimate Tensile Strength**

343 The yield strength (YS) and ultimate tensile strength (UTS) of structural steel can vary with
344 the heat input used during WAAM [88], the heat treatment used (if any) [2], and the angle at
345 which the samples are extracted [75]. These factors lead to a significant variation in both the
346 YS and UTS of steel made by WAAM, as can be seen in Figure 4b and Figure 4c where the
347 YS and UTS data collected from literature (Table 1) are plotted, respectively.

YS and UTS both increase with decreasing linear heat input [88] because lower linear heat inputs lead to smaller melt pools, higher thermal gradients, and therefore faster cooling rates and finer microstructures [97]. The cooling rates found using WAAM are usually a lot faster than those found in conventionally produced parts so the crystalline structure is usually finer [2] and UTS and YS are greater [35]. Classical Hall-Petch grain size strengthening describes why a finer microstructure leads to increased strength; a finer microstructure interrupts dislocation motion more so the yield strength of the material increases [80]. Complex shapes will have different cooling rates at different locations, leading to possible variations in strength across the build [21].

It is likely that there are two competing effects that simultaneously increase and decrease the yield strength with increasing build height. The former effect is caused by the thermal history as the lower layers are effectively annealed, reducing their strength, when further layers are added [80], and the latter by the cooling rate decreasing (hence a coarser microstructure forming) as the layer height increases, due to accumulation of heat [98]. Heat accumulation can occur with geometry changes (e.g. from the wide substrate to the thin wall) as the heat transfer mode changes from mainly conduction, to mainly radiation and convection [99].

Both YS and UTS have been observed to be anisotropic, although to a lesser extent than the Young's modulus [73]. Coupons tested in the 90° orientation have been found to have the lowest YS and UTS [19], whilst those at 45° to the direction of deposition have been found to have the greatest [73], [75]. The former can be explained by the material being loaded across the layers [3], whilst the latter is explained by the 45° samples having the highest density of cell boundaries along the main slip direction [19], [73].

3.4 Ductility

It is essential for structural steels to meet the minimum ductility requirement in order to avoid brittle failure mode. The ductility of structural steel is often measured by the tensile-to-yield strength ratio and the fracture strain, where the two indices are normally positively linked to each other [100]. The ductility requirements for structural carbon steel and stainless steel are the same, as specified in EN 1993-1-1 [100] and EN 1993-1-4 [93].

Using the fracture strain as the index of ductility, Buchanan et al. [3] found that the ductility of WAAM parts is similar to that of conventionally produced parts. However, others have found that the ductility of WAAM parts is often lower than that of wrought or cast components [101] which may be attributed to the fact that the finer microstructure produced by WAAM limits dislocation motion [102]. It was also found that the ductility of the WAAM parts decreases as the yield strength increases (Figure 5a) which is a trend similarly observed for traditionally manufactured structural steels. This may be explained by the fact that the microstructure is affected by the cooling rate, leading to a higher cooling rate being associated with reduced strength and higher ductility [73], [91]. Controlled cooling may be used to obtain the most beneficial microstructure at each location on a build; in the case of a structural beam, the microstructure could be designed such that it provides high strength in the middle of the beam (where there are high forces and moments) but provides higher ductility in connections (where ductility requirements are high) [2]. Cooling can be controlled by introducing a dwell period to reduce the interpass temperature, or by using active cooling (e.g. gases or cryogenics) [35] which can reduce heat accumulation. However, lowering the interpass temperature has the potential to render the production time impractical [82]. Further information on heat accumulation mitigation can be found in [103].

The ductility of WAAM builds can be anisotropic, with reduced ductility perpendicular to the deposition direction due to the elongated anisotropic grains [35], [101]. The effect of heat treatment on the overall ductility of a WAAM build has been debated [104], [105].

The results from literature (Table 1) are compared to the ductility requirements stated in Eurocode 3 [93], [100] in Figure 5, where ε_u is the ultimate strain (corresponding to the ultimate strength σ_u), ε_y it the strain at 0.2% proof stress, and ε_f is elongation at failure. It can be seen that all but two samples met all of the ductility requirements, indicating that WAAM may be capable of producing parts with acceptable ductility for construction purposes. However, Gao et al [106] found that all of their samples had ε_f less than the requirement. No patterns linking the ductility of samples to their angle of extraction are visible, therefore, further research grouping these data by different printing parameters should be carried out to identify any trends.

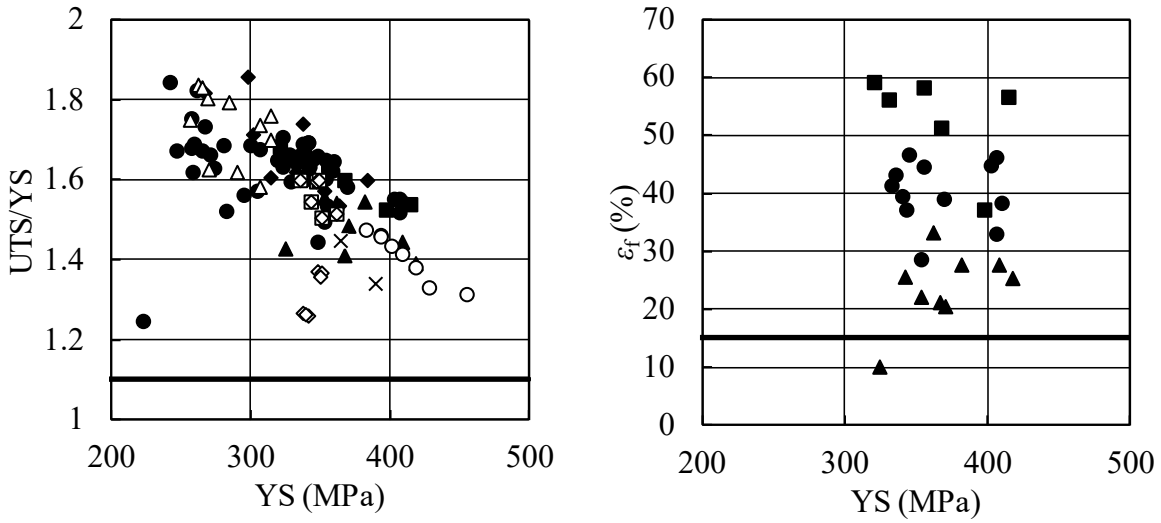

(a) Tensile-to-yield strain ratio UTS/YS

(b) Fracture strain ε_f

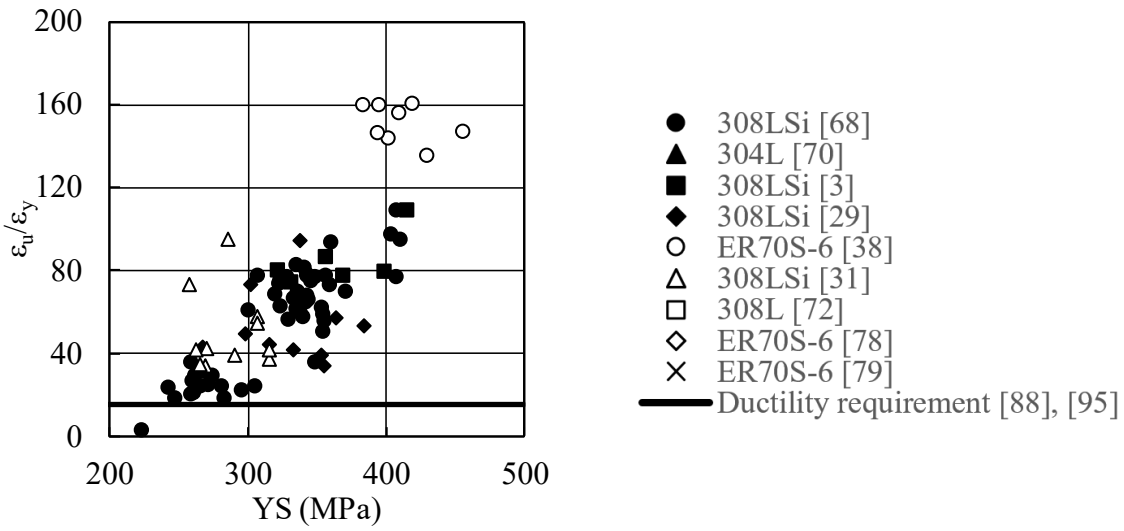

(c) Ultimate tensile strain over yield strain $\varepsilon_u/\varepsilon_y$

Figure 5: WAAM tensile data compared to the ductility requirements in [93], [100]. Permission to use this data has been obtained from the publishers

406

407 **3.5 Fatigue resistance and porosity**

408 WAAM builds are prone to defects such as porosity, and these defects may act as stress
409 concentrators and decrease the fatigue life of the build by up to an order of magnitude compared
410 to that of wrought metals [107]. This is important to consider in cases where fatigue loading
411 can occur (e.g. time dependent winds or rivers hitting bridges) [10]. Different types of porosity
412 are found in WAAM builds including irregular pores (due to shrinkage, lack of
413 binding/fusion/melting or material feed shortage) and spherical pores (due to trapped shielding
414 gas and material evaporation) [101]. Lack of fusion is usually the most detrimental to the
415 fatigue properties due to the elongated shape and sharp corners of the defects [90], and some
416 alloys are more susceptible to this form of defect than others [108]. Heating the substrate is
417 likely to increase lack of fusion porosity [109], and so should be avoided. Porosity can be
418 reduced more by reducing the heat input and by reducing the shield gas flow rate which may
419 also help to reduce the cost of producing large WAAM parts as this has been identified as a

key cost-driver [20]. Results from further porosity analysis on WAAM builds can be found in [103].

Other factors affecting the fatigue life of WAAM builds include the location of the porosity (pores closer to the surface of the build have a greater effect on the fatigue life [110]), the electrical current used (with greater current resulting in reduced porosity) [111], [112], the extent of oxidation [90], and post-processing (including shot peening, machining, and polishing). Shot peening can introduce near surface compressive residual stresses which reduce the susceptibility of cracks to both nucleate and propagate [113], however, it increases the build time as the part must be cooled to a suitable temperature for cold working to be effective [79]. Machined and polished stainless steel 316L WAAM samples have been found to have a fatigue limit (the maximum stress that a material can withstand for an infinite number of stress cycles without breaking) of 260 MPa, whereas just machined samples had a fatigue limit of 250 MPa, and as-built samples had a fatigue limit of 200 MPa [114].

Porosity reduces the ductility of the build [101], however, it is thought that ductility is mainly impaired by the fine microstructure and the residual tensile stresses found in WAAM builds, given that there was no significant increase in strength or ductility when porosity was removed from samples using HIPing [115], [116]. Overall, the fatigue life of WAAM builds can be similar to that of wrought components without post-processing [107], however, the use of WAAM in fatigue-prone applications is debated with some authors suggesting WAAM parts are unlikely to be suitable for fatigue-prone applications without post-processing [2], whilst others have produced more promising results [117].

3.6 Concluding remarks

This section highlights how further research is needed to assess whether the properties achieved through WAAM are acceptable for structural applications. The properties are significantly

affected by the microstructure formed, which in turn is influenced by the processing parameters including heat input, deposition rate, interpass temperature and cooling strategy, direction of build and any ancillary processing. More conclusive results are needed to determine the effect of these parameters, and combinations of them, on the key material properties (Young's modulus, strength and ductility). Analysis into the cost, processing time and environmental impact of WAAM must also be carried out to assess the competitivity of WAAM against traditional manufacturing methods, and how to ensure the process outperforms these traditional methods.

4.0 Geometric properties and structural stability

Parts produced by WAAM without post-machining generally display wavy and rough surfaces along with other geometric imperfections and distortions resulting from welding, making the thickness and overall geometry difficult to characterise. This is significantly different from traditionally fabricated structural steel products where smooth profiles with specified thicknesses are guaranteed by meeting the corresponding geometric requirements (e.g. [118]). When first developed in the Mechanical Engineering sector, WAAM products were first produced into raw shapes with wavy surfaces and then further machined into the desired exact geometry, especially for components subject to high-cycle fatigue [52], [119], [120]. This led to designs including a machining allowance of additional material [121]. Depending on the material and welding techniques, the surface waviness of the build may vary. Numerous efforts have been made to optimise process parameters in order to produce surfaces as smooth as possible. This has been done primarily for expensive alloys e.g. titanium [52], [122]–[124] and aluminium [28], [41], [125]–[127], with relatively little investigation for stainless steel and other constructional steel types (e.g. carbon steel). However, constructional products are generally much larger than the scale of the amplitude of the surface waviness, therefore may

be subjected to relaxed requirements on the geometric accuracy. Nevertheless, the surface quality and geometrical precision must be understood as they affect the characterisation of the design resistance and the material efficiency of WAAM construction [29]. In this section, common geometric imperfections, including surface roughness, surface waviness, humping, geometric distortion, and balling [88] in WAAM structures are reviewed and the influences of manufacturing parameters on them are discussed.

4.1 Surface roughness

Surface roughness is defined as the average height of a peak or depth of a trough across the surface [90] and can occur within layers (Figure 6a). Surface roughness of WAAM stainless steel parts and carbon steel parts generally fall between 0.135-0.57 mm, as a result of process parameters chosen in previous works [4], [50], [128], [129]. Although the overall stability of steel structures may be hardly affected by the surface roughness due to its relatively small scale compared to the part's overall dimension, it is important to minimise the surface roughness as it introduces stress concentrations that can act as crack nucleation sites (i.e. the notch effect), limiting the fatigue life of the build [90].

Factors influencing the surface roughness may include the power of the heat source, the travel speed, the layer height (typically 1-2 mm [4]), overhang angles and scan strategy. These may lead to the "stair step effect" (when a curved or inclined surface is approximated by layers rather than being smooth) and balling (see Section 4.3), which are the two main causes of surface roughness. The former cause is affected by the build angle and layer height, with thinner layers reducing roughness but increasing built time [90]. These undulations can be milled away to avoid non-uniform deformation [3] but this is an expensive and time-consuming process, and the rough finish can be beneficial when producing composites [2]. Surface roughness may also be reduced by a hybrid additive/subtractive processing; for example, the

top surface of the deposited material could be milled flat before the next layer is added, improving surface roughness and geometrical accuracy [130].

4.2 Surface waviness

Surface waviness is defined as shown in Equation 1, where the effective wall width is the width after machining away all undulations (Figure 6b), whilst minimising the amount of material removed. It usually occurs on a larger scale/at a lower frequency than surface roughness (across layers – Figure 6b) and it is attributed to the variations in the size of the melt pool (and therefore bead geometry [131]) and so can be heavily effected by variations in the heat input [88]. Surface waviness can also be caused by spatter [120] and can lead to cross-section shape irregularities (Figure 6b) [50] and stress concentration similar to the notch effect [132].

In mechanical applications, the surface waviness is associated with material efficiency as it represents the amount of material to be removed to eliminate surface irregularities [133], however, machining away the surface waviness is not a desired process in construction applications. The surface waviness must still be kept to a minimum as greater surface waviness correlates to a smaller effective thickness, potentially reducing the structural resistance and material efficiency of WAAM builds. Current design treatment, as proposed by some researchers [73], includes obtaining the material properties from unmachined coupons, which implicitly accounts for the influence of surface waviness on the stiffness and strength of the walls. Others [128] found that using the averaged 'effective' thickness as the reference to calculate the structural resistance of WAAM stub columns also gives closer estimation to the theoretical values given in Eurocode 3 [93], [100].

$$\text{Surface waviness} = \frac{\text{Total wall thickness} - \text{Effective wall thickness}}{2} \quad (1)$$

For constructional metals such as stainless steels and carbon steels, the WAAM builds have a typical surface waviness ranging from 0.18 mm to 0.78 mm [134], [135]. Although it is difficult

to rule out the surface waviness completely in WAAM construction, it may be improved by adjusting the process parameters that affect the size of the melt pool, including the heat input used, with a lower heat input resulting in narrower melt pools [88]. Further details of melt pools and bead geometry can be found in [77], [131], [136], [137].

4.3 Humping

Humping occurs when the scanning speed is too fast; the molten pool becomes elongated and can become unstable, breaking up into puddles of liquid instead of remaining as a single pool [90]. This results in a discontinuity of the deposited geometry and a non-uniform thickness of the build in the scanning direction [138]. The humping effects accumulated along building height may create a texture pattern at a certain angle to the substrate (Figure 6c). This can lead to anisotropic behaviour in the stiffness and strength of unmachined walls [139], imposing difficulty in characterising its geometry for structural resistance prediction and deteriorating the material efficiency of the builds. Therefore, it is important for engineers to balance the economic benefit from fast fabrication with the extent of humping deemed acceptable in structural design, as well as being able to characterise the effect during the design.

4.4 Geometric distortion

Thin-walled metal parts produced by WAAM may show deviations to the target geometry due to material shrinkage and distortion [103], [140], leading to geometric imperfections such as lack-of-straightness and/or cross-sectional distortions (Figure 6e) [29]. One major reason for geometric distortion may be attributed to the residual stresses from welding, which can occur in WAAM structures due to shrinkage on cooling (largest in the direction of deposition). Resulting tensile stresses can be a source of solidification and HAZ (heat affected zone) cracking [90], delamination [141], and distortion (which can drive crack nucleation and growth) [101]. This can alter the contact tip distance which can affect the quality of deposition, leading

to geometric imperfections and stress concentrations [35]. The lack of straightness can generate load eccentricities on walls thereby affecting their resistances to the loading conditions they were designed for. For example, the stub columns tested by Laghi et. al. [29] were subject to a combination of compression and bending due to their irregular shape (Figure 6e and f).

Shrinkage and distortion may be alleviated by altering the process parameters including increasing interpass temperature and/or reducing the heat input. The heat input is given by Equation 2, highlighting how increasing the travel speed, and/or decreasing the voltage and/or current may decrease the extent of shrinkage and distortion [142]. However, these adjustments to the process parameters may entail tedious trial-and-error compensation, will affect the size of the melt pool and can compromise corrosion and fatigue resistance [35]. Post processing treatment such as heat treatment [2] may also improve residual stress related distortions. To compensate the shrinkage and distortion, a novel method exploiting thermo-mechanical finite element modelling and correcting the CAD geometry to define the welding path, has been proposed and validated for thin-walled WAAM parts [143] with improved accuracy.

$$\text{Heat input} = \frac{\text{Voltage} \times \text{Current}}{\text{Travel speed}} \tag{2}$$

Other strategies to reduce the geometric distortion may include adopting symmetrical or back-to-back builds [4], improved scan strategies [50], mechanically tensioning the substrate and intermediately rolling the deposits [144], [145], although these strategies have mainly been used with non-steel metals such as aluminium and titanium alloys. Side rolling has been proved to be more effective than vertical rolling at reducing residual stress and distortion, but it requires supports for thin walls [146]. Support structures can reduce distortion by constraining the part mechanically and by transferring heat to the substrate, reducing residual stresses but increasing the volume of material used [33].

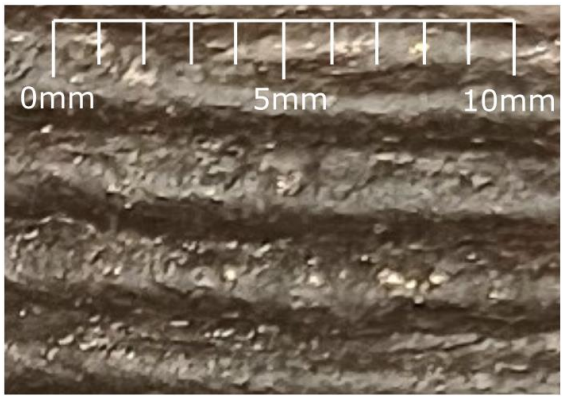

a) Surface roughness within layers (image by authors).

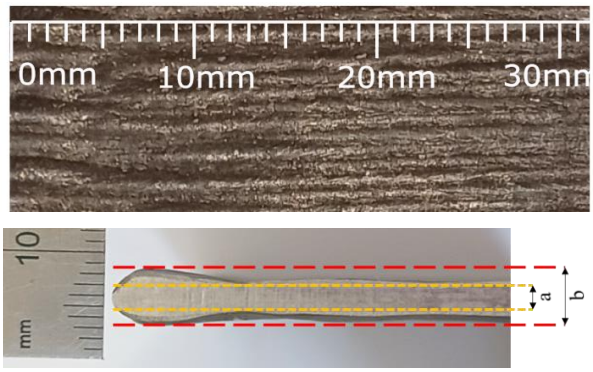

b) Top: Surface waviness between layers. Bottom: Surface waviness, a – effective thickness, b – total thickness (images by authors).

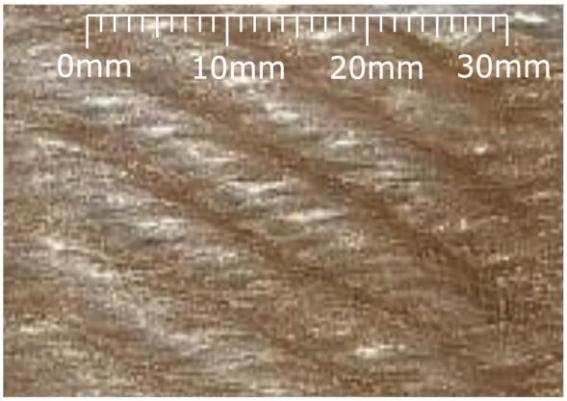

c) Humping with a pattern at an angle (image by authors).

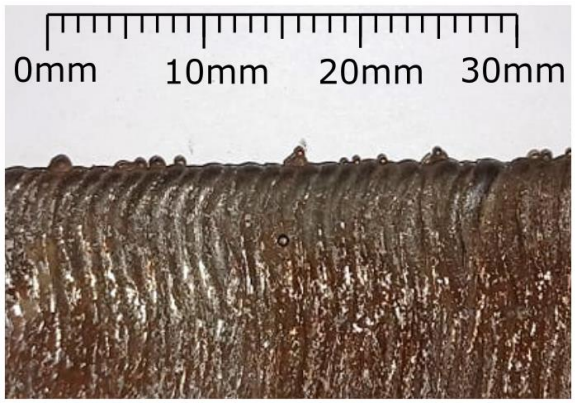

d) Balling (image by authors).

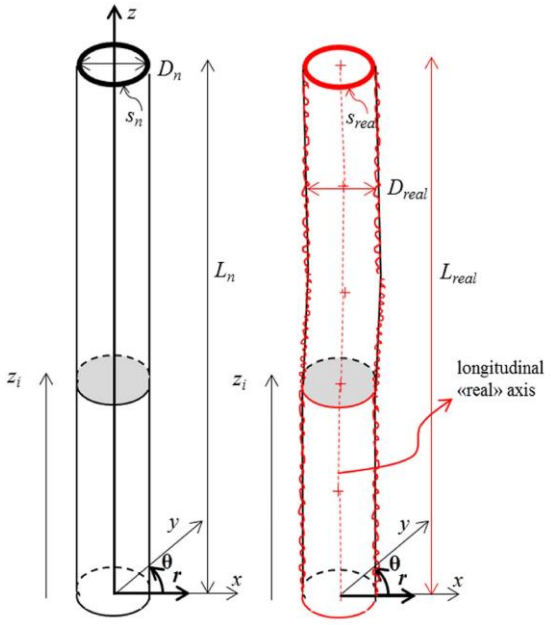

e) Out-of-straightness shown by the deviation of the longitudinal axis of a member (reprinting permission for these images has been obtained from the publisher [29]).

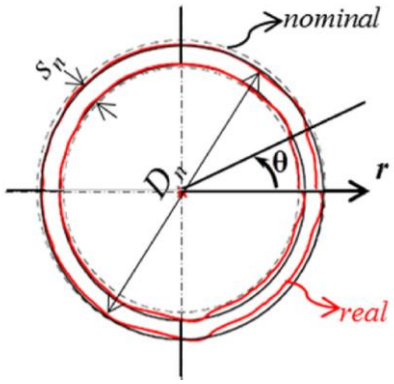

f) Cross-section distorsion shown by diviations in thickness and diameter (reprinting permission for these images has been obtained from the publisher [29]).

Figure 6: Typical geometric imperfections of WAAM builds.

562 Greater residual stresses require more robust and expensive fixing to constrain the part,
563 negating the benefits of "tool-less" manufacturing using AM [35]. A stiffer substrate will
564 reduce the amount of distortion, but will increase the residual stresses and if these exceed the
565 yield stress of the feedstock, cracking may be observed along the grain boundaries [90]. In
566 general, high levels of residual stress should be avoided, unless the residual stress is in the
567 opposite sense of the load applied (i.e. prestressing) [2].

568 **4.5 Balling**

569 Balling is a phenomenon that occurs when the liquid material fails to wet the substrate/previous
570 layer due to surface tension, and so it spheroidizes (Figure 6d). The presence of balling
571 increases the material waste, as it does not contribute to the structural resistance of the WAAM
572 parts, and it should be ignored in design. However, in experimental research, balling can lead
573 to inaccurate measurement of the geometric dimensions. The noises created by balling in 3D
574 scanned geometric data may be trimmed off computationally or removed physically by
575 polishing [128]. However, balling should be generally avoided when selecting the fabrication
576 parameters, including minimising contamination and oxidation, the main causes of balling
577 phenomenon [65].

578 **4.6 Structural stability**

579 There is limited knowledge regarding the structural response of WAAM structures [75] as
580 current research mainly focusses on the microstructural and metallurgical properties of builds,
581 rather than explicit investigation for construction purposes [22]. The overall buckling
582 resistance of WAAM structures can be affected by a combination of material and geometric
583 imperfections. To this end, a few initial stub column tests of WAAM structures are collected
584 and discussed in this section. Tests on circular hollow section (CHS) stub columns have been
585 carried out, demonstrating that the non-negligible initial out-of-straightness of the specimens

586 can lead to a combination of compression and bending [19], [29], [66]. Tests on square hollow
587 section (SHS) stub columns have also been carried out, in particular to verify the compressive
588 structural response of the MX3D bridge, with Class 1 and Class 4 sections being tested to
589 determine the effects of local buckling. Results show that Class 1 CHS specimens underwent
590 more strain hardening than SHS specimens. Eurocode 3 provisions do not currently take strain
591 hardening into account, and the extent of strain hardening suggests that design provisions
592 specific to WAAM may be required [19], [51].

593 The available test results of steel SHS and EAS stub columns made by WAAM [51],[128] are
594 plotted and compared against the EC 3 design curves for internal and outstand plates [93] in
595 Figures 7 and 8, respectively. In Figures 7 and 8, the horizontal axis is slenderness , calculated
596 using Equations 3 and 4, where k_σ is the buckling factor corresponding to the stress ratio and
597 boundary conditions (here taken as k_σ = 4 for SHS [93] and 1.28 for the tested EAS stub
598 columns [128]), and E and $\sigma_{0.2}$ are taken from the relevant tensile coupon tests in 90° direction
599 [51],[128]. The vertical axis of Figures 7 and 8 is the normalised buckling resistance $N_u/A\sigma_{0.2}$,
600 where N_u is the maximum load attained during the test and A is the average cross-sectional area.

$$\bar{\lambda}_p = \frac{c/t}{28.4\varepsilon\sqrt{k_\sigma}} \tag{3}$$

$$\varepsilon = \left[\frac{235}{\sigma_{0.2}}\frac{E}{210000}\right]^{0.5} \tag{4}$$

601

602 In Figure 7, the WAAM AISI 308LSi stainless steel SHS data [51] has been manipulated to
603 give the slenderness and normalised buckling resistances based on different material properties,
604 as obtained from as-built and machined tensile coupon tests. Test data from conventionally
605 produced AISI 304 stainless steel sections [147] is also included in for comparison purposes.
606 Figure 7 demonstrates that the effective width equation can mostly be met if the as-built tensile

test values are used, and that it mostly can't if the machined tensile test values are used, highlighting the need for standards when designing WAAM structures using Eurocode 3 provisions. It also shows that the resistances of these WAAM sections are less than that of the traditional manufacturing methods and as expected, an increase in the local slenderness leads to a reduction in the normalised capacity of the section.

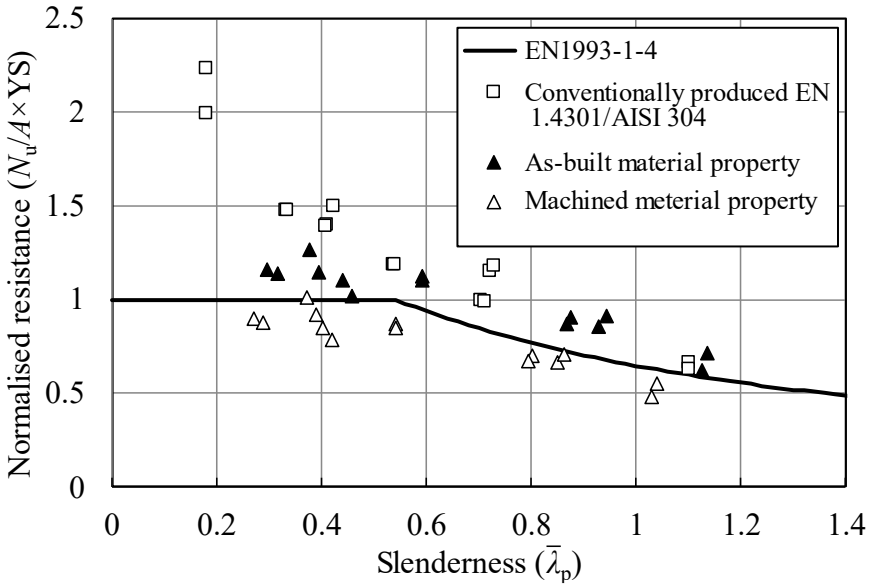

Figure 7: Local buckling resistance of stiffened stainless steel plates (tested by square hollow sections stub columns) produced by different manufacturing processes (conventionally produced *[147]* and WAAM [51]) with the design equation in EN 1993-1-4 *[93]*.

Instead of using the 'as-built' material properties as suggested by [51], Figure 8 employs the material properties obtained from machined tensile coupons and offers an alternative way of characterisating the stability performance of WAAM plates. Two types of thickness definitions are compared: one is the 'average' thickness (defined as the total volume of the stub column over column height and plate width [51]), and the other one is the 'effective' thickness (defined as the average of the minimum thicknesses of each layer of deposition [128]). As demonstrated in Figure 8, using the effective thickness in calculations results in a stability performance of WAAM parts closer to the Eurocode characterisation.

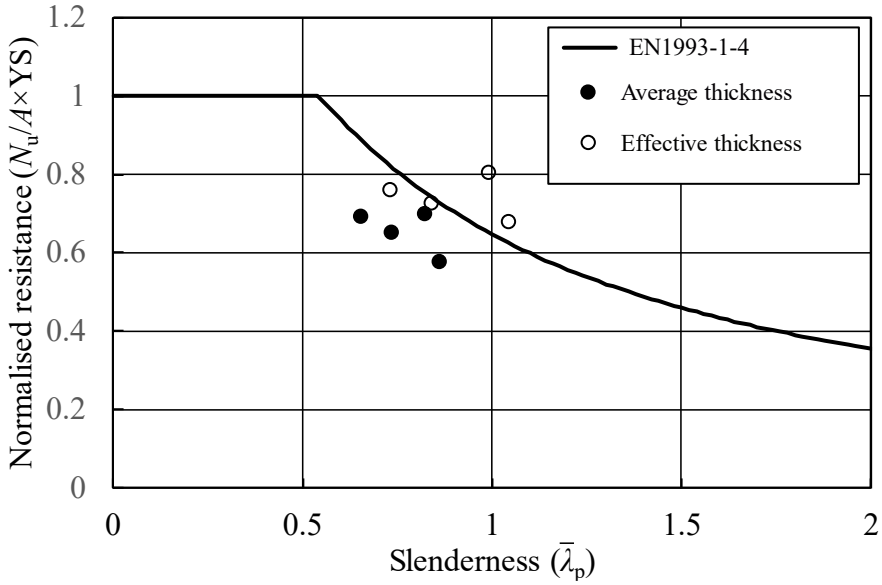

Figure 8: Local buckling resistance of unstiffened stainless steel plates (tested by equal angle section stub columns produced by WAAM *[128]*), with the Eurocode 3 design equation *[93]*.

4.7 Concluding remarks

The various geometric imperfections which can occur in WAAM builds have been discussed, including surface roughness, surface waviness, humping, balling, and geometric distortion. Mitigation and post-processing methods have been suggested, however, detailed analysis on the effect of these defects on the strucutural stability of WAAM builds has been rare, requiring further research. The available experimental results demonstrated that the provisions given in Eurocode 3 for structural stability may be met by WAAM builds depending on the material properties (i.e. as-built or machined) and geometric dimensions (i.e. avarage wall-thickness or effective wall thickness) used in calculations.

5.0 Design

Applications of WAAM in construction may vary from basic structural elements, beams and columns [29], [50], [51], truss members [16], [148], connections (e.g. plated hooks [149], bolted nodes [149] and joints for spatial shells [31]), to whole-piece self-standing structures (e.g. bridges [18], [19]). In addition to the stability design of basic plated elements made by

WAAM as discussed in section 4, this section focuses on reviewing advanced structural optimisation methods to design free-form but efficient shapes that can fully exploit the advantages of WAAM. The precedent design cases adopt different structural optimisation techniques as a result of both the manufacturing constraints and the structural requirements, learning from which, a range of structural optimisation techniques tailored to WAAM construction are discussed in this section.

5.1 Optimisation with wall thickness constraint

Complex shapes containing both solid parts and thin-walled elements are achievable thanks to advances in path-planning and manufacturing process control (Section 2). Nevertheless, majority of previous construction applications of WAAM [18], [19], [29], [51] adopted thin-walled design with constant thicknesses to facilitate an easy manufacturing process. The manufacturing constraints determine the form of the structure which may be designed by different optimisation techniques, which can be grouped as continuum topology optimisation, discrete topology optimisation and shape optimisation.

WAAM parts designed by continuum topology optimisation may be limited by both a minimum feature size (as a result of the welding nozzle size) and a maximum feature size (to minimise the large residual stresses and distortion which can be generated in large-volume parts). The minimum feature size control has been extensively investigated and research is comparatively mature. It is initially achieved by the filtering scheme within the framework of density-based topology optimisation [150]. A method for robust control of minimum feature size can be found in [151]. Control of the maximum feature size can be realized by restricting the material volume within the neighbouring region of each element [152], [153]. Based on maximum and minimum feature size control techniques, a method that can impose uniform feature size to the optimal topology has been proposed [154], which is particularly applicable

667 to WAAM structures. The continuum topology optimisation methods may be suitable for
668 design connections [155] and structural members [154] (Figure 9).

669

(a) A connection [155] (b) A cantilever beam [154]

670 Figure 9: Examples of structural parts designed by topology optimisation (reprinting
671 permission for these images has been obtained from the publisher *[154], [155]*).

672

673 Discrete topology optimisation techniques may be combined with post-processing methods to
674 design gridshell structures. An end-to-end framework to bridge structural optimization with
675 WAAM has been proposed in [151]. In this framework, truss topology optimisation was first
676 adopted to determine the overall geometry and member size of the truss. Cross-section design
677 was then performed to generate different cross-section sizes by varying the diameter whilst
678 maintaining a constant wall thickness. The truss joints were then designed by a post-processing
679 treatment to allow a feasible manufacturing path (Figure 3a). Discrete topology optimisation
680 can be also used in combination with 'dot to dot' welding mode to allow free-form grided shell
681 structures/skeletons to be designed (Figure 10) [156].

682 Shape optimisation may be suitable for designing cross-section shapes that are subject to in-
683 plane loading, and continuum roof shells that are subject to out-of-plane loading. An
684 optimisation method was adopted to find a free-form cross-section shape with optimised local
685 buckling resistance (Figure 11a) [157]. Shape optimisation of continuum shell structures has

been reported in [158], where the optimal structures can sustain the out-of-plane bending actions by in-plane membrane force (Figure 11b).

Figure 10: An example of a gridshell structure (a bike frame) made by a ‘dot-to-dot’ mode of welding using WAAM (reprinting permission for this image has been obtained from the publisher *[156]*).

(a) Reference stainless steel circular shell and optimized, Aster and wavy shells 3D printed by powder bed fusion (reprinting permission for these images has been obtained from the publisher [157]).

(b) Shape optimisation of a sheet subject to out-of-plane loads (reprinting permission for these images has been obtained from the publisher [158]).

Figure 11: Examples of shape optimisation of steel shells and plates with fixed thicknesses

5.2 Optimisation with constraints on build directions and overhangs

WAAM builds inevitably have anisotropic material properties due to the fact that solidification occurs under a thermal gradient in this layer-by-layer process [159]. This kind of anisotropy can be exploited to maximize the structural stiffness by simultaneously optimizing the structural layout and deposition directions [65][160]. Another consideration of the anisotropic behaviour can be seen from the optimization of the printing direction. Significant steps towards characterising this anisotropy have been made in [159].

WAAM with multi-axis platforms and the ability to perform horizontal welding (although with compromised quality), may be less affected by the constraints of overhang structures. However, supporting structure may be still needed due to the limited space for the welding torch and the connectivity of the structures. The presence of supporting structure necessitates the removal process, which might delay the manufacturing process. In a worst-case scenario, supporting structures may locate within the enclosed internal voids, being impossible to remove after the complete of the printing jobs. To avoid the use of supporting structures, extra material can be added to those regions that display overly large overhang angles, to meet the overhang limits [161]. Otherwise, the overhang constraints can be considered together with topology optimization. A method that can impose a minimum allowable self-supporting angle in the optimal topology is developed within the topology optimization framework such that designed components and structures are adequately supported from below is found in [162]. The avoidance of supporting structures can also be achieved by excluding the unprintable geometries from the design space during topology optimization process, in this way, fully self-supporting optimized designs can be obtained [163].

5.3 Concluding remarks

This section discussed various structural optimisation techniques tailored to WAAM builds, including topology optimisations based on continuum and discrete structures, as well as shape optimisation based on structures with constant wall thicknesses, in response to the fact that most WAAM constructions to date have adopted constant wall thicknesses with a single pass of welding. Manufacturing constraints such as nozzle size, structural overhang and material anisotropy that need to be considered in the structural optimisation have also been discussed.

6.0 Conclusions and further research suggestions

This review details the major research areas related WAAM in construction, including manufacturing techniques, material properties, geometry, structural response, and design. These research areas have gained the attention of many research groups and companies alike. Although recent builds demonstrate the potential of WAAM in construction, there are numerous research gaps and areas for future investigation, described as follows.

6.1 Standardization of manufacturing process

Since the general standard ASTM 52900 (defining the terminology and acronyms commonly used in AM) was developed and published in 2015 [164], more specific standards have been created, in particular for DED [165], [166]and PBF [167]. However, there are currently no standardised manufacturing processes for building steel structures using WAAM, as the process parameters have been mainly governed by the geometric accuracy and printability. This has resulted in different research groups and manufacturers using different wire thicknesses, welding machines, robot systems and energy sources. The required material properties, surface finishes (i.e. machined or as-built) and geometric accuracy for construction applications need to be specified before the manufacturing processes can be standardised. Furthermore, it is currently difficult to justify the economic benefit of WAAM construction

against the traditional steel manufacturing and construction route. Research may be performed to investigate the possibility of adopting a higher deposition rate to get the cost down so that it can attract more applications. It is also likely that new manufacturing standards will need to be created to cover structural components made by AM [10]. This could then lead to reduced safety margins needed in design [10]. Novel manufacturing processes may also be explored to increase the quality and productivity for WAAM in construction, including hybrid energy sources, in-process treatments and scanning strategies, etc.

6.2 Stability performance

There is limited research into the structural response of WAAM structures because the testing completed is primarily material testing. The materials tested were mainly stainless steels, with other constructional steel types (e.g. mild carbon steel, high strength steel and aluminium) barely investigated. Upon the standardisation of manufacturing processes, material properties and geometric accuracy, the stability performance of WAAM structures must be investigated by more structural testing on various constructional steel types. In addition, the surface finishes that are highly related to structural stability needs to be characterised and used to determine whether it is necessary to machine the WAAM parts. Based on the results of these tests, reliable design rules for WAAM structures may be proposed. The design provisions included in Eurocodes 3 are unlikely to be suitable for WAAM structures due to their greater geometric variability, so these provisions will have to be adapted.

6.3 Application scenarios and design

Due to its relatively slow building speed compared to traditional manufacturing methods and high energy cost, WAAM construction is still facing challenges in justifying its economic and energy efficiencies against traditional structural steel construction, which is already a mature industry with manufacturing, design and construction methods developed. A complete life

cycle analysis of the printing process needs to be carried out to assess the environmental impact of producing structures this way. Innovative application scenarios where WAAM outweighs the traditional construction need to be explored, including but not being limited to, innovative structural forms with greater material efficiency (e.g. structurally optimised components), fabrication of complicated connections (e.g. multi-axis joints of various section shapes), being used in conjunction of 'green' construction materials (e.g. connections to timber structures), reinforcement cage of 'free-form' concrete structures, and automotive construction. In addition to the reviewed structural optimisation techniques, more integrated design procedures considering all manufacturing aspects/process constrains of WAAM need to be established.

Declaration of Competing Interest

The authors declare that they have no known competing financial interests or personal relationships that could have appeared to influence the work reported in this paper.

Acknowledgements

The authors would like to acknowledge support from BRE for the PhD studentship.

References

[1] European Commission, Executive Agency for Small and Medium-sized Enterprises, B. Pedersen, L. Probst, and J. Wenger, *Skills for smart industrial specialisation and digital transformation : final report*. Publications Office, 2019. doi: 10.2826/117803.

[2] C. Buchanan and L. Gardner, ‘Metal 3D printing in construction: A review of methods, research, applications, opportunities and challenges’, *Engineering Structures*, no. 180, pp. 332–348, Feb. 2019.

[3] C. Buchanan, W. Wan, and L. Gardner, ‘Testing of Wire and Arc Additively Manufactured Stainless Steel Material and Cross-Sections’, Hong Kong, China, Dec. 2018.

[4] S. W. Williams, F. Martina, A. C. Addison, J. Ding, G. Pardal, and P. Colegrove, ‘Wire + Arc Additive Manufacturing’, *Materials Science and Technology*, vol. 32, no. 7, pp. 641–647, May 2016, doi: 10.1179/1743284715Y.0000000073.

[5] H. Tang, M. Qian, N. Liu, X. Zhang, G. Yang, and J. Wang, ‘Effect of powder reuse times on additive manufacturing of Ti-6Al-4V by selective electron beam melting’, *Jom*, vol. 67, no. 3, pp. 555–563, 2015.

[6] J. O. Milewski, ‘Lasers, Electron Beams, Plasma Arcs’, in *Additive Manufacturing of Metals*, Springer, 2017, pp. 85–97.

[7] B. Berman, ‘3-D printing: The new industrial revolution | Elsevier Enhanced Reader’, 2012. https://reader.elsevier.com/reader/sd/pii/S0007681311001790?token=199782179396344AA0E35E069E9CEA2CF2990895F0F97CDE4F812F1CB1D48AE56216843239449D79DBF2059208131D37 (accessed Nov. 07, 2020).

[8] F. Martina and S. Williams, ‘Wire+arc additive manufacturing vs. traditional machining from solid: a cost comparison’, Cranfield University, 2015.

[9] ‘World Steel in Figures’, World Steel Association, Belgium, 2020.

[10] A. Kanyilmaz *et al.*, ‘Role of metal 3D printing to increase quality and resource-efficiency in the construction sector’, *Additive Manufacturing*, vol. 50, 2022.

[11] E. Costa, P. Shepherd, J. Orr, T. Ibell, and R. Oval, ‘Automating Concrete Construction: Digital Design of Non-prismatic Reinforced Concrete Beams’, in *Second RILEM International Conference on Concrete and Digital Fabrication*, Cham, 2020, pp. 863–872.

[12] A. Paolini, S. Kollmannsberger, and E. Rank, ‘Additive manufacturing in construction: A review on processes, applications and digital planning methods’, *Additive Manufacturing*, vol. 30, 2019.

[13] P. A. Kobryn and S. L. Semiatin, ‘Mechanical Properties of Laser-Deposited Ti-6Al-4V’, Wright-Patterson Air Force Base, 2001.

[14] S. Keating, J. Leland, L. Cai, and N. Oxman, ‘Toward site-specific and seld-sufficient robotic fabrication on architectural scales’, *Science Robotics*, vol. 2, no. 5, 2017.

[15] N. Labonnote, A. Ronnquist, B. Manum, and P. Ruther, ‘Additive construction: State-of-the-art, challenges and opportunities | Elsevier Enhanced Reader’, 2016. https://reader.elsevier.com/reader/sd/pii/S0926580516301790?token=FC630803A42A9E90453BE407748E1B81A17DF25B8F2EB9F654EB01DAB5711E318D8AEE72913F737FCB8FD99E30C3FF8E (accessed Nov. 07, 2020).

[16] J. Ye, P. Kyvelou, F. Gilardi, H. Lu, M. Gilbert, and L. Gardner, ‘An End-to-End Framework for the Additive Manufacture of Optimizes Tubular Structures’, *IEEE*, 2021.

[17] ‘Connector for Takenaka’, *MX3D*. https://mx3d.com/industries/construction/connector-for-takenaka/ (accessed May 03, 2022).

[18] T. Feucht, J. Lange, B. Waldschmitt, AK. Schudlich, M. Klein, and M. Oechsner, ‘Welding Process for the Additive Manufacturing of Cantilevered Components with the WAAM’, in *Advanced Joining Processes*, vol. 125, Singapore: Springer, 2020.

[19] L. Gardner, P. Kyvelou, G. Herbert, and C. Buchanan, ‘Testing and initial verification of the world’s first metal 3D printed bridge’, *Journal of Constructional Steel Research*, no. 172, p. 106233, 2020.

[20] C. R. Cunningham *et al.*, ‘Cost Modelling and Sensitivity Analysis of Wire and Arc Additive Manufacturing’, *Procedia Manufacturing*, vol. 11, pp. 650–657, Jan. 2017, doi: 10.1016/j.promfg.2017.07.163.

[21] C. R. Cunningham, J. M. Flynn, A. Shokrani, V. Dhokia, and S. T. Newman, ‘Invited review article: Strategies and processes for high quality wire arc additive manufacturing’, *Additive Manufacturing*, vol. 22, pp. 672–686, 2018.

[22] V. Laghi, M. Palermo, G. Gasparini, V. Girelli, and T. Trombetti, ‘Geometrical Characterization of Wire-and-Arc Additive Manufactured Steel Elements’, *Advanced Materials Letters*, vol. 10, no. 10, pp. 695–699, 2019.

[23] Y. K. Bandari, S. W. Williams, J. Ding, and F. Martina, ‘Additive manufacture of large structures: robotic or CNC systems?’, 2015.

[24] A. Khorasani, I. Gibson, J. K. Veetil, and A. H. Ghasemi, ‘A review of technological improvements in laser-based powder bed fusion of metal printers’, *The International Journal of Advanced Manufacturing Technology*, vol. 108, pp. 191–209, 2020.

[25] F. Careri, S. Imbrogno, D. Umbrello, M. M. Attallah, J. Outeiro, and A. C. Batista, ‘Machining and heat treatment as post-processing strategies for Ni-superalloys structures fabricated using direct energy deposition’, *Journal of Manufacturing Processes*, vol. 61, pp. 236–244, 2021.

[26] R. Kuhne, M. Feldmann, S. Citarelli, U. Reisgen, R. Sharma, and L. Oster, ‘3D printing in steel construction with automated Wire Arc Additive Manufacturing’, Copenhagen, Denmark, Sep. 2019.

[27] L. Wang, J. Xue, and Q. Wang, ‘Correlation between arc mode, microstructure, and mechanical properties during wire arc additive manufacturing of 316L stainless steel’, *Materials Science & Engineering A*, no. 751, pp. 183–190, 2019.

[28] Y. Yehorov, L. da Silva, and A. Scotti, ‘Balancing WAAM Production Costs and Wall Surface Quality through Parameter Selection: A Case Study of an Al-Mg5 Alloy Multilayer-Non-Oscillated Single Pass Wall’, *Journal of Manufacturing and Materials Processing*, vol. 3, no. 2, 2019.

[29] V. Laghi, M. Palermo, G. Gasparini, V. Girelli, and T. Trombetti, ‘Experimental results for structural design of Wire-and-Arc Additive Manufactured stainless steel members’, *Journal of Constructional Steel Research*, vol. 167, 2020, [Online]. Available: https://doi.org/10.1016/j.jcsr.2019.105858

[30] J. Wang, M. Evernden, B. Chater, and J. Pan, ‘Printing imperfections – geometric patterns to improve resistances of 3D printed steel plates’, *ce/papers*, vol. 4, no. 2–4, pp. 1822–1828, Sep. 2021, doi: 10.1002/cepa.1491.

[31] V. Laghi, M. Palermo, M. Pragliola, V. Girelli, G. Van Der Velden, and T. Trombetti, ‘Towards 3D-printed steel grid-shells: the main idea and first studies’, Boston, USA, Jul. 2018.

[32] A. Nycz, A. I. Adediran, M. W. Noakes, and L. J. Love, ‘Large Scale Metal Additive Techniques Review’, Manufacutring Systems Research, Oak Ridge National Laboratory, Knoxville, 2016.

[33] C. Buchanan, V. Matilainen, A. Salminen, and L. Gardner, ‘Structural performance of additive manufactured metallic material and cross-sections’, *Journal of Constructional Steel Research*, no. 136, pp. 35–48, 2017, doi: 10.1016/j.jcsr.2017.05.002.

[34] E. Brandl, C. Leyens, and F. Palm, ‘Mechanical Properties of Additive Manufactured Ti-6Al-4V Using Wire and Powder Based Processes’, 2011, vol. 26.

[35] C. R. Cunningham, J. Wang, V. Dhokia, A. Shrokani, and S. T. Newman, ‘Characterisation of Austenitic 316LSi Stainless Steel Produced by Wire Arc Additively Manufacturing with Interlayer Cooling’, Austin, USA, 2019.

[36] F. Xu *et al.*, ‘Realisation of a multi-sensor framework for process monitoring of the wire arc additive manufacturing in producing Ti-6Al-4V parts’, *null*, vol. 31, no. 8, pp. 785–798, Aug. 2018, doi: 10.1080/0951192X.2018.1466395.

[37] D. Ding, Z. Pan, D. Cuiuri, and H. Li, ‘Wire-feed additive manufacturing of metal components: technologies, developments and future interests’, *The International Journal of Advanced Manufacturing Technology*, vol. 81, pp. 465–481, 2015.

[38] H. Xin, I. Tarus, L. Cheng, M. Veljkovic, N. Persem, and L. Lorich, ‘Experiments and numerical simulation of wire and arc additive manufactured steel materials’, *Structures*, vol. 34, pp. 1393–1402, 2021.

[39] D. H. Phillips, ‘2.1 Fundamentals and Principles of Arc Welding’, in *Welding Engineering - An Introduction*, Joh Wiley & Sons, 2016.

[40] P. M. Sequeira Almeida and S. W. Williams, ‘Innovative process model of Ti-6Al-4V additive layer manufacturing using cold metal transfer (CMT)’, Austin, 2010.

[41] C. G. Pickin and K. Young, ‘Evaluation of cold metal transfer (CMT) process for welding aluminium alloy’, *Science and Technology of Welding and Joining*, vol. 11, no. 5, pp. 583–585, 2006.

[42] G. Lorenzin and G. Rutili, ‘The innovative use of low heat input in welding: experiences on “cladding” and brazing using the CMT process’, *Welding International*, vol. 23, no. 8, pp. 622–632, 2009.

[43] F. Martina, J. Mehnen, S. W. Williams, P. Colegrove, and F. Wang, 'Investigation of the benefits of plasma deposition for the additive layer manufacture of Ti-6Al-4V', *Journal of Materials Processing Technology*, vol. 212, no. 6, pp. 1377–1386, 2012.

[44] T. Abe and H. Sasahara, 'Layer geometry control for the fabrication of lattice structures by wire and arc additive manufacturing', *Additive Manufacturing*, vol. 28, pp. 639–648, Aug. 2019, doi: 10.1016/j.addma.2019.06.010.

[45] A. Ščetinec, D. Klobčar, and D. Bračun, 'In-process path replanning and online layer height control through deposition arc current for gas metal arc based additive manufacturing', *Journal of Manufacturing Processes*, vol. 64, pp. 1169–1179, Apr. 2021, doi: 10.1016/j.jmapro.2021.02.038.

[46] J. Xiong, Y. Zhang, and Y. Pi, 'Control of deposition height in WAAM using visual inspection of previous and current layers', *Journal of Intelligent Manufacturing*, vol. 32, no. 8, pp. 2209–2217, Dec. 2021, doi: 10.1007/s10845-020-01634-6.

[47] B. Xu *et al.*, 'Shape-driven control of layer height in robotic wire and arc additive manufacturing', *Rapid Prototyping Journal*, vol. 25, no. 10, pp. 1637–1646, Jan. 2019, doi: 10.1108/RPJ-11-2018-0295.

[48] Y. Wang *et al.*, 'Coordinated monitoring and control method of deposited layer width and reinforcement in WAAM process', *Journal of Manufacturing Processes*, vol. 71, pp. 306–316, Nov. 2021, doi: 10.1016/j.jmapro.2021.09.033.

[49] C. Xia *et al.*, 'Model predictive control of layer width in wire arc additive manufacturing', *Journal of Manufacturing Processes*, vol. 58, pp. 179–186, Oct. 2020, doi: 10.1016/j.jmapro.2020.07.060.

[50] V. Laghi, M. Palermo, G. Gasparini, V. Girelli, and T. Trombetti, ‘On the influence of the geometrical irregularities in the mechanical response of Wire-and-Arc Additively Manufactured planar elements’, *Journal of Constructional Steel Research*, vol. 178, 2021.

[51] P. Kyvelou, C. Huang, L. Gardner, and C. Buchanan, ‘Structural Testing and Design of Wire Arc Additively Manufactured Square Hollow Sections’, *Journal of Structural Engineering*, vol. 147, no. 12, 2021.

[52] Z. Pan, D. Ding, B. Wu, D. Cuiuri, H. Li, and J. Norrish, ‘Arc Welding Processes for Additive Manufacturing: A Review’, *Transactions on Intelligent Welding Manufacturing, Springer, Singapore*, pp. 3–24, 2018.

[53] T. A. Rodrigues, V. Duarte, R. M. Miranda, T. G. Santos, and J. P. Oliveira, ‘Current Status and Perspectives on Wire and Arc Additive Manufacturing (WAAM)’, *Materials*, vol. 12, no. 7, 2019, doi: 10.3390/ma12071121.

[54] Y. Feng, B. Zhan, J. He, and K. Wang, ‘The double-wire feed and plasma arc additive manufacturing process for deposition in Cr-Ni stainless steel’, *Journal of Materials Processing Technology*, vol. 259, pp. 206–215, 2018.

[55] M. A. Somashekara, M. Naveenkumar, A. Kumar, C. Viswanath, and Simhambhatla, ‘Investigations into effect of weld-deposition pattern on residual stress evolution for metallic additive manufacturing’, *The International Journal of Advanced Manufacturing Technology*, vol. 90, pp. 2009–2025, 2017.

[56] J. Shi, F. Li, S. Chen, Y. Zhao, and H. Tian, ‘Effect of in-process active cooling on forming quality and efficiency of tandem GMAW–based additive manufacturing’, *The International Journal of Advanced Manufacturing Technology*, vol. 101, no. 5, pp. 1349–1356, Apr. 2019, doi: 10.1007/s00170-018-2927-4.

[57] F. Martina, J. Ding, S. Williams, A. Caballero, G. Pardal, and L. Quintino, ‘Tandem metal inert gas process for high productivity wire arc additive manufacturing in stainless steel’, *Additive Manufacturing*, vol. 25, pp. 545–550, Jan. 2019, doi: 10.1016/j.addma.2018.11.022.

[58] F. Michel, H. Lockett, J. Ding, F. Martina, G. Marinelli, and S. Williams, ‘A modular path planning solution for Wire + Arc Additive Manufacturing’, *Robotics and Computer-Integrated Manufacturing*, vol. 60, pp. 1–11, Dec. 2019, doi: 10.1016/j.rcim.2019.05.009.

[59] C. Wang, W. Suder, J. Ding, and S. Williams, ‘Wire based plasma arc and laser hybrid additive manufacture of Ti-6Al-4V’, *Journal of Materials Processing Technology*, vol. 293, 2021.

[60] C. Wang, W. Suder, J. Ding, and S. Williams, ‘Bead shape control in wire based plasma arc and laser hybrid additive manufacture of Ti-6Al-4V’, *Journal of Manufacturing Processes*, vol. 68, no. Part A, pp. 1849–1859, Aug. 2021.

[61] J. Ding *et al.*, ‘Thermo-mechanical analysis of Wire and Arc Additive Layer Manufacturing process on large multi-layer parts’, *Computational Materials Science*, vol. 50, no. 12, pp. 3315–3322, 2011.

[62] J. Xiong, G. Zhang, J. Hu, and Y. Li, ‘Forecasting process parameters for GMAW-based rapid manufacturing using closed-loop iteration based on neural network’, *The International Journal of Advanced Manufacturing Technology*, vol. 69, no. 1, pp. 743–751, Oct. 2013, doi: 10.1007/s00170-013-5038-2.

[63] J. Qin *et al.*, ‘Research and application of machine learning for additive manufacturing’, *Additive Manufacturing*, vol. 52, p. 102691, Apr. 2022, doi: 10.1016/j.addma.2022.102691.

[64] A. Diourté, F. Bugarin, C. Bordreuil, and S. Segonds, ‘Continuous three-dimensional path planning (CTPP) for complex thin parts with wire arc additive manufacturing’, *Additive Manufacturing*, vol. 37, p. 101622, Jan. 2021, doi: 10.1016/j.addma.2020.101622.

[65] M. Bruggi, V. Laghi, and T. Trombetti, ‘Simultaneous design of the topology and the build orientation of Wire-and-Arc Additively Manufactured structural elements’, *Computers and Structures*, vol. 242, 2021.

[66] R. Zhang, L. Gardner, C. Buchanan, V. Matilainen, H. Piili, and A. Salminen, ‘Testing and analysis of additively manufactured stainless steel CHS in compression’, *Thin-Walled Structures*, vol. 159, 2021.

[67] D. Ding, Z. Pan, D. Cuiuri, and H. Li, ‘A practical path planning methodology for wire and arc additive manufacturing of thin-walled structures’, *Robotics and Computer-Integrated Manufacturing*, vol. 34, pp. 8–19, Aug. 2015, doi: 10.1016/j.rcim.2015.01.003.

[68] N. Grossi, A. Scippa, G. Venturini, and G. Campatelli, ‘Process Parameters Optimization of Thin-Wall Machining for Wire Arc Additive Manufactured Parts’, *Applied Sciences*, vol. 10, no. 21, 2020, doi: 10.3390/app10217575.

[69] J. G. Lopes, C. M. Machado, V. R. Duarte, T. A. Rodrigues, T. G. Santos, and J. P. Oliveira, ‘Effect of milling parameters on HSLA steel parts produced by Wire and Arc Additive Manufacturing (WAAM)’, *Journal of Manufacturing Processes*, vol. 59, pp. 739–749, Nov. 2020, doi: 10.1016/j.jmapro.2020.10.007.

[70] G. Campatelli, F. Montevecchi, G. Venturini, G. Ingarao, and P. C. Priarone, ‘Integrated WAAM-Subtractive Versus Pure Subtractive Manufacturing Approaches: An Energy Efficiency Comparison’, *International Journal of Precision Engineering and Manufacturing-Green Technology*, vol. 7, no. 1, pp. 1–11, Jan. 2020, doi: 10.1007/s40684-019-00071-y.

[71] S. Zhang, Y. Zhang, M. Gao, F. Wang, Q. Li, and X. Zeng, ‘Effects of milling thickness on wire deposition accuracy of hybrid additive/subtractive manufacturing’, *null*, vol. 24, no. 5, pp. 375–381, Jul. 2019, doi: 10.1080/13621718.2019.1595925.

[72] H. Nagamatsu, H. Sasahara, Y. Mitsutake, and T. Hamamoto, ‘Development of a cooperative system for wire and arc additive manufacturing and machining’, *Additive Manufacturing*, vol. 31, p. 100896, Jan. 2020, doi: 10.1016/j.addma.2019.100896.

[73] P. Kyvelou *et al.*, ‘Mechanical and microstructural testing of wire and arc additively manufactured sheet material’, *Materials & Design*, no. 192, p. 108675, 2020.

[74] L. Ji, J. Lu, C. Liu, H. Fan, and S. Ma, ‘Microstructure and mechanical properties of 304L steel fabricated by arc additive manufacturing’, 2017, vol. 128.

[75] V. Laghi, M. Palermo, L. Tonelli, G. Gasparini, L. Ceschini, and T. Trombetti, ‘Tensile properties and microstructural features of 304L austenitic stainless steel produced by wire-and-arc additive manufacturing’, *The International Journal of Advanced Manufacturing Technology*, no. 106, pp. 3693–3705, 2020.

[76] I. Tarus, H. Xin, M. Veljkovic, N. Persem, and L. Lorich, ‘Evaluation of material properties of 3D printed carbon steel for material modelling’, *ce/papers*, vol. 4, no. 2–4, pp. 1650–1656, 2021.

[77] V. T. Le, D. S. Mai, T. K. Doan, and H. Paris, ‘Wire and arc additive manufacturing of 308L stainless steel components: Optimization of processing parameters and material properties’, *Engineering Science and Technology, an International Journal*, vol. 24, pp. 1015–1026, 2021.

[78] J. V. Gordon, C. V. Haden, H. F. Nied, R. P. Vinci, and D. G. Harlow, ‘Fatigue crack growth anisotropy, texture and residual stress in austenitic steel made by wire and arc additive manufacturing’, *Materials Science & Engineering A*, no. 724, pp. 431–438, 2018.

[79] C. R. Cunningham, V. Dhokia, and S. T. Newman, ‘Effects on in-process LN2 cooling on the microstructre and mechanical properties of type 316L stainless steel produced by wire arc directed energy deposition’, *Materials Letters*, vol. 282, 2021.

[80] C. V. Haden, G. Zeng, F. M. Carter III, C. Ruhl, B. A. Krick, and D. G. Harlow, ‘Wire and arc additive manufactured steel: Tensile and wear properties’, *Additive Manufacturing*, no. 16, pp. 115–123, 2017.

[81] C. R. Cunningham, ‘Pulse Metal Inert Gas based Wire Arc Additive Manufacturing of an Austenitic Stainless Steel’, PhD, University of Bath, 2020.

[82] E. Aldalur, F. Veiga, A. Suárez, J. Bilbao, and A. Lamikiz, ‘High deposition wire arc additive manufacturing of mild steel: Strategies and heat input effect on microstructure and mechanical properties’, *Journal of Manufacturing Processes*, vol. 58, pp. 615–626, Oct. 2020, doi: 10.1016/j.jmapro.2020.08.060.

[83] V. T. Le, ‘A preliminary study on gas metal arc welding-based additive manufacturing of metal parts’, *Science & Technology Development Journal*, vol. 23, no. 1, pp. 422–429, 2020, doi: 10.32508/stdj.v23i1.1714.

[84] A. Ermakova, A. Mehmanparast, S. Ganguly, J. Razavi, and F. Berto, ‘Investigation of mechanical and fracture properties of wire and arc additively manufactured low carbon steel components’, *Theoretical and Applied Fracture Mechanics*, vol. 109, p. 102685, Oct. 2020, doi: 10.1016/j.tafmec.2020.102685.

[85] W. Jin, C. Zhang, S. Jin, Y. Tian, D. Wellmann, and W. Liu, ‘Wire Arc Additive Manufacturing of Stainless Steels: A Review’, 2020.

[86] H. L. Wei, J. Mazumder, and T. DebRoy, ‘Evolution of solidification texture during additive manufacturing’, *Scientific Reports*, 2015.

[87] J. Wang *et al.*, 'Grain morphology evolution and texture characterization of wire and arc additive manufactured Ti-6Al-4V', *Journal of Alloys and Compounds*, vol. 768, pp. 97–113, May 2018.

[88] Q. Wu, Z. Ma, G. Chen, C. Liu, D. Ma, and S. Ma, 'Obtaining fine microstructure and unsupported overhangs by low heat input pulse arc additive manufacturing', *Journal of Manufacturing Processes*, no. 27, pp. 198–206, 2017.

[89] M. J. Bermingham, D. H. StJohn, J. Krynen, S. Tedman-Jones, and M. S. Dargusch, 'Promoting the columnar to equiaxed transition and grain refinement of titanium alloys during additive manufacturing', *Acta Materialia*, no. 168, pp. 261–274, 2019.

[90] T. DebRoy *et al.*, 'Additive manufacturing of metallic components - Process, structure and properties', *Progress in Materials Science*, no. 92, pp. 112–224, 2018.

[91] K. Wang, D. Wang, and F. Han, 'Effect of crystalline grain structure on the mechanical properties of twinning-induced plasticity steel', *Theoretical and Applied Mechanics Letters*, vol. 32, no. 1, pp. 181–187, 2016.

[92] P. Liu, Z. Wang, Y. Xiao, M. Horstemeyer, X. Cui, and L. Chen, 'Insight into the mechanisms of columnar to equiaxed grain transition during metallic additive manufacturing', *Additive Manufacturing*, no. 26, pp. 22–29, 2019, doi: 10.1016/j.addma.2018.12.019.

[93] European Committee for Standardization (CEN), 'Eurocode 3: Design of steel structures. Part 1-4: General rules - Supplementary rules for stainless steels', Brussels, Belgium, EN 1993-1-4, 2006.

[94] J. R. Davis, *Stainless Steels*. ASM International, 1994.

[95] 'Stainless Steel - Grade 308L (UNS S30880)', *AZoM.com*, Feb. 26, 2013. https://www.azom.com/article.aspx?ArticleID=8205 (accessed Mar. 25, 2022).

[96] ‘ASTM-A240: Standard for Chromium and Chromium-Nickel Stainless Steel Plate, Sheet and Strip’. ASTM, 2004. [Online]. Available: https://shspecialsteel.com/wp-content/uploads/2020/01/ASTM-A240-Standard-for-Chromium-and-Chromium-Nickel-Stainless-Steel-Plate-Sheet-and-Strip.pdf

[97] E. O. Hall, ‘The Deformation and Ageing of Mild Steel: III Discussion of Results’, *Proceedings of the Physical Society. Section B*, vol. 64, pp. 747–753, 1951.

[98] V. D. Manvatkar, A. A. Gokhale, G. Jagen Reddy, A. Venkataramana, and A. De, ‘Estimation of Melt Pool Dimensions, Thermal Cycle, and Hardness Distribution in the Laser-Engineered Net Shaping Process of Austenitic Stainless Steel’, *Metallurgical and Materials Transactions*, vol. 42, no. 13, pp. 4080–4087, 2011.

[99] J. Wang, Q. Sun, H. Wang, J. Liu, and J. Feng, ‘Effect of location on microstructure and mechanical properties of additive layer manufactured Inconel 625 using gas tungsten arc welding’, *Materials Science and Engineering: A*, vol. 676, pp. 395–405, 2016.

[100] European Committee for Standardization (CEN), ‘Eurocode 3: Design on steel structures. Part 1-1: General rules and rules for buildings’, Brussels, Belgium, EN 1993-1-1, 2005.

[101] D. Bourell *et al.*, ‘Materials for additive manufacturing’, *CIRP Annals - Manufacturing Technology*, no. 66, pp. 659–681, 2017.

[102] O. Panchenko, D. Kurushkin, I. Mushnikov, A. Khismatullin, and A. Popovich, ‘A high-performance WAAM process for Al-Mg-Mn using controlled short-circuiting metal transfer at increased wire feed rate and increased travel speed’, *Materials & Design*, vol. 195, 2020.

[103] D. Jafari, T. H. J. Vaneker, and I. Gibson, ‘Wire and arc additive manufacturing: Opportunities and challenges to control the quality and accuracy of manufactured parts’, *Materials & Design*, vol. 202, p. 109471, Apr. 2021, doi: 10.1016/j.matdes.2021.109471.

[104] E. Brandl, B. Baufeld, C. Leyens, and R. Grault, ‘Additive manufactured Ti-6Al-4V using welding wire: comparison of laser and arc beam deposition and evaluation with respect to aerospace material specifications’, *Physics Procedia*, vol. 5, pp. 595–606, 2010.

[105] M. J. Bermingham, D. Kent, H. Zhang, D. H. StJohn, and M. S. Dargusch, ‘Controlling the microstructure and properties of wire arc additive manufactured Ti-6Al-4V with trace boron additions’, *Acta Materialia*, vol. 91, pp. 289–303, 2015.

[106] C. Gao, X. Chen, C. Su, and X. Chen, ‘Location dependence of microstructure and mechanical properties on wire arc additively manufactured nuclear grade steel’, *Vacuum*, vol. 168, p. 108818, Oct. 2019, doi: 10.1016/j.vacuum.2019.108818.

[107] J. Gordon, J. Hochhalter, C. Haden, and D. Harlow, ‘Enhancement in fatigue performance of metastable austenitic stainless steel through directed energy deposition additive manufacturing’, *Materials and Design*, no. 168, 2019.

[108] T. Mukherjee, J. S. Zuback, A. De, and T. DebRoy, ‘Printability of alloys for additive manufacturing’, *Scientific Reports*, vol. 6, no. 19717, 2016.

[109] S. Siddique, M. Imran, E. Wycisk, C. Emmelmann, and F. Walther, ‘Influence of process-induced microstructure and imperfections onmechanical properties of AlSi12 processed by selective laser melting’, *Journal of Materials Processing Technology*, no. 221, pp. 205–213, 2015.

[110] A. Fatemi, R. Molaei, S. Sharifimehr, N. Phan, and N. Shamsaei, ‘Multiaxial fatigue behavior of wrought and additive manufacturedTi-6Al-4V including surface finish effect’, *International Journal of Fatigue*, no. 100, pp. 347–366, 2017.

[111] K. Pal and S. Pal, ‘Effect of Pulse Parameters on Weld Quality in Pulsed Gas Metal Arc Welding: A Review’, *Journal of Materials Engineering and Performance*, vol. 20, pp. 918–931, 2011.

[112] P. K. Ghosh, S. R. Gupta, P. C. Gupta, and R. Rathi, ‘Fatigue characteristics of pulsed MIG-welded Al-Zn-Mg alloy’, *Journal of Materials Science*, vol. 26, pp. 6161–6170, 1991.

[113] E. Salvati *et al.*, ‘Eigenstrain reconstruction of residual strains in an additively manufactured and shot peened nickel superalloy compressor blade’, *Computer Methods in Applied Mechanics and Engineering*, vol. 320, pp. 335–351, 2017.

[114] A. B. Spierings, T. L. Starr, and K. Wegener, ‘Fatigue performance of additive manufactured metallic parts’, *Rapid Prototyping Journal*, vol. 19, no. 2, pp. 88–94, 2013.

[115] M. J. Bermingham, L. Nicastro, D. Kent, Y. Chen, and M. S. Dargusch, ‘Optimising the mechanical properties of Ti-6Al-4V components produced by wire + arc additive manufacturing with post-process heat treatments’, *Journal of Alloys and Compounds*, no. 753, pp. 247–255, 2018.

[116] S. Leuders *et al.*, ‘On the mechanical behaviour of titanium alloy TiAl6V4 manufactured by selective laser melting: Fatigue resistance and crack growth performance’, *International Journal of Fatigue*, no. 48, pp. 300–307, 2013.

[117] H. Bartsch, R. Kühne, S. Citarelli, S. Schaffrath, and M. Feldmann, ‘Fatigue analysis of wire arc additive manufactured (3D printed) components with unmilled surface’, *Structures*, vol. 31, pp. 576–589, Jun. 2021, doi: 10.1016/j.istruc.2021.01.068.

[118] European Committee for Standardization (CEN), ‘BS EN 10219-2 Cold-formed welded structural hollow sections of non-alloy and fine grain steels. Part 2: Tolerances, dimensions and sectional properties’. 2006.

[119] S. Williams and F. Martina, ‘Wire + arc additive manufacturing vs. traditional machining from solid: a cost comparison’, Welding Engineering and Laser Processing Centre, Cranfield University, 2015.

[120] C. Fuchs, D. Baier, T. Semm, and M. F. Zaeh, ‘Determining the machining allowance for WAAM parts’, *Production Engineering*, vol. 14, no. 5, pp. 629–637, Dec. 2020, doi: 10.1007/s11740-020-00982-9.

[121] B. Stucker and X. Qu, ‘A finish machining strategy for rapid manufactured parts and tools’, *Rapid Prototyping Journal*, vol. 9, no. 4, pp. 194–200, Jan. 2003, doi: 10.1108/13552540310489578.

[122] J. Liu, Y. Xu, Y. Ge, Z. Hou, and S. Chen, ‘Wire and arc additive manufacturing of metal components: a review of recent research developments’, *The International Journal of Advanced Manufacturing Technology*, vol. 111, pp. 149–198, 2020.

[123] Y. Zhuo *et al.*, ‘Grain refinement of wire arc additive manufactured titanium alloy by the combined method of boron addition and low frequency pulse arc’, *Materials Science and Engineering: A*, vol. 805, p. 140557, Feb. 2021, doi: 10.1016/j.msea.2020.140557.

[124] P. A. Colegrove *et al.*, ‘High Pressure Interpass Rolling of Wire + Arc Additively Manufactured Titanium Components’, *Advanced Materials Research*, vol. 996, pp. 694–700, 2014, doi: 10.4028/www.scientific.net/AMR.996.694.

[125] S. Srivatsav, V. Jayakumar, and M. Sathishkumar, ‘Recent developments and challenges associated with wire arc additive manufacturing of Al alloy: A review’, *Materials Today: Proceedings*, 2021.

[126] K. S. Derekar, ‘A review of wire arc additive manufacturing and advances in wire arc additive manufacturing of aluminium’, *Materials Science and Technology*, 2018.

[127] K. Derekar, J. Lawrence, G. Melton, A. Addison, X. Zhang, and L. Xu, 'Influence of Interpass Temperature on Wire Arc Additive Manufacturing (WAAM) of Aluminium Alloy Components', *MATEC Web Conf.*, vol. 269, 2019, doi: 10.1051/matecconf/201926905001.

[128] S. I. Evans and J. Wang, 'Material Properties and Local Stability of WAAM Stainless Steel Plates With Different Deposition Rates (Submitted)', Chengdu, China, May 2022.

[129] J. Xiong, Y.-J. Li, Z.-Q. Yin, and H. Chen, 'Determination of Surface Roughness in Wire and Arc Additive Manufacturing Based on Laser Vision Sensing', *Chinese Journal of Mechanical Engineering*, vol. 31, no. 1, p. 74, Aug. 2018, doi: 10.1186/s10033-018-0276-8.

[130] H. L. Wei, H. K. D. H. Bhadeshia, S. A. David, and T. DebRoy, 'Harnessing the scientific synergy of welding and additive manufacturing', *Science and Technology of Welding and Joining*, vol. 24, no. 5, pp. 361–366, 2019, doi: 10.1080/13621718.2019.1615189.

[131] J. H. Park, M. Cheepu, and S. M. Cho, 'Analysis and Characterization of the Weld Pool and Bead Geometry of Inconel 625 Super-TIG Welds', *Metals*, vol. 10, no. 3, 2020, doi: 10.3390/met10030365.

[132] K. Samadian and W. Waele, 'Fatigue Crack Growth Model Incorporating Surface Waviness For Wire+Arc Additively Manufactured Components', *Procedia Structural Integrity*, vol. 28, pp. 1846–1855, 2020.

[133] A. Busachi, J. Erkoyuncu, P. Colegrove, F. Martina, and J. Ding, 'Designing a WAAM Based Manufacturing System for Defence Applications', *Procedia CIRP*, vol. 37, pp. 48–53, Jan. 2015, doi: 10.1016/j.procir.2015.08.085.

[134] P. Dirisu, G. Supriyo, F. Martina, X. Xu, and S. Williams, ‘Wire plus arc additive manufactured functional steel surfaces enhanced by rolling’, *International Journal of Fatigue*, vol. 130, p. 105237, Jan. 2020, doi: 10.1016/j.ijfatigue.2019.105237.

[135] V. R. Duarte, T. A. Rodrigues, N. Schell, T. G. Santos, J. P. Oliveira, and R. M. Miranda, ‘Wire and Arc Additive Manufacturing of High-Strength Low-Alloy Steel: Microstructure and Mechanical Properties’, *Advanced Engineering Materials*, vol. 23, no. 11, p. 2001036, Nov. 2021, doi: 10.1002/adem.202001036.

[136] M. Dinovitzer, X. Chen, J. Laliberte, X. Huang, and H. Frei, ‘Effect of wire and arc additive manufacturing (WAAM) process parameters on bead geometry and microstructure’, *Additive Manufacturing*, vol. 26, pp. 138–146, Mar. 2019.

[137] X. Ding, Y. Koizumi, D. Wei, and C. Akihiko, ‘Effect of process parameters on melt pool geometry and microstructure development for electron beam melting of IN718: A systematic single bead analysis study’, *Additive Manufacturing*, vol. 26, pp. 215–226, 2019.

[138] L. Yuan *et al.*, ‘Investigation of humping phenomenon for the multi-directional robotic wire and arc additive manufacturing’, *Robotics and Computer-Integrated Manufacturing*, vol. 63, p. 101916, Jun. 2020, doi: 10.1016/j.rcim.2019.101916.

[139] H. Geng, J. Li, J. Xiong, X. Lin, and F. Zhang, ‘Geometric Limitation and Tensile Properties of Wire and Arc Additive Manufacturing 5A06 Aluminum Alloy Parts’, *Journal of Materials Engineering and Performance*, vol. 26, no. 2, pp. 621–629, 2017.

[140] L. Nguyen, J. Buhl, R. Israr, and M. Bambach, ‘Analysis and compensation of shrinkage and distortion in wire-arc additive manufacturing of thin-walled curved hollow sections’, *Additive Manufacturing*, vol. 47, p. 102365, Nov. 2021, doi: 10.1016/j.addma.2021.102365.

[141] Q. Wu, T. Mukherjee, C. De, and T. DebRoy, ‘Residual stresses in wire-arc additive manufacturing - Hierarchy of influential variables’, *Additive Manufacturing*, vol. 35, 2020.

[142] A. Wu, D. W. Brown, M. Kumar, G. Gallegos, and W. King, ‘An Experimental Investigation into Additive Manufacturing-Induced Residual Stresses in 316L Stainless Steel’, *Metallurgical and Materials Transactions A*, vol. 45, pp. 6260–6270, 2014.

[143] C. Cambon, S. Rouquette, I. Bendaoud, C. Bordreuil, R. Wimpory, and F. Soulie, ‘Thermo-mechanical simulation of overlaid layers made with wire + arc additive manufacturing and GMAW-cold metal transfer’, *Welding in the World*, vol. 64, no. 8, pp. 1427–1435, Aug. 2020, doi: 10.1007/s40194-020-00951-x.

[144] P. A. Colegrove *et al.*, ‘Microstructure and residual stress improvement in wire and arc additively manufactured parts through high-pressure rolling’, *Journal of Materials Processing Technology*, vol. 213, no. 10, pp. 1782–1791, Oct. 2013, doi: 10.1016/j.jmatprotec.2013.04.012.

[145] F. Martina *et al.*, ‘Residual stress of as-deposited and rolled wire+arc additive manufacturing Ti-6Al-4V components’, *Materials Science and Technology*, vol. 32, no. 14, pp. 1439–1448, 2016, doi: 10.1080/02670836.2016.114270410.1080/02670836.2016.1142704.

[146] P. Colegrove and S. Ganguly, ‘Residual stress characterization and control in the additive manufacture of large scale metal structures’, *Residual Stresses 2016*, p. 455, 2017.

[147] L. Gardner and D. A. Nethercot, ‘Experiments on stainless steel hollow sections - Part 1: Material and cross-sectional behaviour’, *Journal of Constructional Steel Research*, vol. 60, no. 9, pp. 1291–1318, 2004.

[148] T. Wang, X. Zhou, and H. Zhang, ‘Control of forming process of truss structure based on cold metal transition technology’, *Rapid Prototyping Journal*, vol. 28, no. 2, pp. 204–215, Jan. 2022, doi: 10.1108/RPJ-12-2020-0314.

[149] J. Lange, T. Feucht, and M. Erven, ‘3D printing with steel’, *Steel Construction*, vol. 13, no. 3, pp. 144–153, Aug. 2020, doi: 10.1002/stco.202000031.

[150] O. Sigmund, ‘Design of material structures using topology optimization’, 1994.

[151] F. Wang, B. S. Lazarov, and O. Sigmund, ‘On projection methods, convergence and robust formulations in topology optimization’, *Structural and Multidisciplinary Optimization*, vol. 43, no. 6, pp. 767–784, Jun. 2011, doi: 10.1007/s00158-010-0602-y.

[152] E. Fernández, M. Collet, P. Alarcón, S. Bauduin, and P. Duysinx, ‘An aggregation strategy of maximum size constraints in density-based topology optimization’, *Structural and Multidisciplinary Optimization*, vol. 60, no. 5, pp. 2113–2130, Nov. 2019, doi: 10.1007/s00158-019-02313-8.

[153] J. K. Guest, ‘Imposing maximum length scale in topology optimization’, *Structural and Multidisciplinary Optimization*, vol. 37, no. 5, pp. 463–473, Feb. 2009, doi: 10.1007/s00158-008-0250-7.

[154] E. Fernández, C. Ayas, M. Langelaar, and P. Duysinx, ‘Topology optimisation for large-scale additive manufacturing: generating designs tailored to the deposition nozzle size’, *Virtual and Physical Prototyping*, vol. 16, no. 2, pp. 196–220, Mar. 2021, doi: 10.1080/17452759.2021.1914893.

[155] H. Seifi, A. Rezaee Javan, S. Xu, Y. Zhao, and Y. M. Xie, ‘Design optimization and additive manufacturing of nodes in gridshell structures’, *Engineering Structures*, vol. 160, pp. 161–170, Apr. 2018, doi: 10.1016/j.engstruct.2018.01.036.

[156] ‘Dutch Students Create a Unique 3D Printed Metal Bicycle with Help from MX3D’, *3DPrint.com | The Voice of 3D Printing / Additive Manufacturing*, Feb. 03, 2016. https://3dprint.com/118086/dutch-students-3d-printed-bike/ (accessed May 03, 2022).

[157] R. Zhang *et al.*, *Optimisation and compressive testing of additively manufactured stainless steel corrugated shells*, vol. 4. 2021, p. 1836. doi: 10.1002/cepa.1492.

[158] M. Firl, R. Wüchner, and K.-U. Bletzinger, ‘Regularization of shape optimization problems using FE-based parametrization’, *Struct Multidisc Optim*, vol. 47, no. 4, pp. 507–521, Apr. 2013, doi: 10.1007/s00158-012-0843-z.

[159] N. Hadjipantelis, B. Weber, C. Buchanan, and L. Gardner, ‘Description of anisotropic material response of wire and arc additively manufactured thin-walled stainless steel elements’, *Thin-Walled Structures*, vol. 171, p. 108634, Feb. 2022, doi: 10.1016/j.tws.2021.108634.

[160] V. Mishra, C. Ayas, M. Langelaar, and F. van Keulen, ‘Simultaneous topology and deposition direction optimization for Wire and Arc Additive Manufacturing’, *Manufacturing Letters*, vol. 31, pp. 45–51, Jan. 2022, doi: 10.1016/j.mfglet.2021.05.011.

[161] M. Leary, L. Merli, F. Torti, M. Mazur, and M. Brandt, ‘Optimal topology for additive manufacture: A method for enabling additive manufacture of support-free optimal structures’, *Materials & Design*, vol. 63, pp. 678–690, Nov. 2014, doi: 10.1016/j.matdes.2014.06.015.

[162] A. T. Gaynor and J. K. Guest, ‘Topology optimization considering overhang constraints: Eliminating sacrificial support material in additive manufacturing through design’, *Structural and Multidisciplinary Optimization*, vol. 54, no. 5, pp. 1157–1172, Nov. 2016, doi: 10.1007/s00158-016-1551-x.

[163] M. Langelaar, ‘Topology optimization of 3D self-supporting structures for additive manufacturing’, *Additive Manufacturing*, vol. 12, pp. 60–70, Oct. 2016, doi: 10.1016/j.addma.2016.06.010.

[164] ‘BS EN ISO/ASTM 52900:2017 Additive Manufacturing - General Principles - Terminology’. BSI Standards Publication, 2017.

[165] ASTM International, ‘ASTM F3187-16 Standard Guide for Directed Energy Deposition of Metals’. 2016.

[166] SAE, ‘AMS7005 - Wire fed plasma arc directed energy deposition additive manufacturing process’. 2019.

[167] SAE, ‘AMS7003 - Laser Powder Bed Fusion Process’. 2018.